Advanced Control of Switched Reluctance Motors (SRMs): A Review on Current Regulation, Torque Control and Vibration Suppression

GAOLIANG FANG [1] (Student Member, IEEE), **FILIPE P. SCALCON** [2] (Student Member, IEEE),
DIANXUN XIAO [1] (Student Member, IEEE), **RODRIGO P. VIEIRA** [2] (Member, IEEE),
HILTON A. GRÜNDLING [2] (Member, IEEE), AND **ALI EMADI** [1] (Fellow, IEEE)

[1] McMaster Automotive Resource Center (MARC), McMaster University, Hamilton, ON L8P 0A6, Canada
[2] Power Electronics and Control Research Group, Federal University of Santa Maria, Santa Maria, RS 97105-900, Brazil

CORRESPONDING AUTHOR: FILIPE PINARELLO SCALCON (e-mail: filipescalcon1@gmail.com)

ABSTRACT With the increasing environmental concerns, a paradigm shift towards electric and hybrid electric vehicles is expected. Switched Reluctance Motors (SRMs) have emerged as a viable competitor to other established electrical machines. SRMs are known for their simple construction, robustness, inherent fault tolerant structure and low production and maintenance costs. Moreover, the machine has gained interest due to the absence of permanent magnets or windings in the rotor structure, which significantly reduces production costs when compared to other electric motors. The SRM, however, present some known drawbacks, such as increased torque ripple and acoustic noise production, as well as a highly nonlinear behavior. Through the use of adequate control strategies, however, the main challenges of the machine can be overcome. Thus, this paper presents a state-of-the-art review of the advanced control of SRMs, encompassing current regulation strategies, torque control strategies and vibration suppression techniques. First, two categories of current controllers are reviewed: model-independent and model-based. Next, indirect and direct torque control methods are explored. Then, three approaches to vibration suppression are discussed, namely active cancellation, current profiling and direct instantaneous force control. Lastly, a summary of each topic is presented and suggestions of future research topics are listed.

INDEX TERMS Current regulation, switched reluctance motor, torque control, torque ripple, vibration suppression.

I. INTRODUCTION

Due to the increasing concerns surrounding fossil fuels and global warming, significant efforts have been made in recent years towards transportation electrification. Electric vehicles (EVs) and hybrid EVs have been attracting much attention, specially due to increasing governmental support programs. Permanent magnet synchronous motors (PMSMs) are often used for EV applications, given they present high efficiency and superior power density when compared to other electric motors [1]–[5]. However, rare-earth materials, used in the production of permanent magnets, present some disadvantages, such as high cost and irreversible demagnetization in high-temperature conditions. Moreover, the mining and extraction of rare-earth materials also presents significant environmental concerns [6]. Thus, the development of high-performance electric drives that do not rely on rare-earth magnets has received great attention in recent years [7]–[10].

In this context, switched reluctance motors (SRMs) stand out as a solid competitor for already established electrical machines, being a rare-earth-free alternative. SRMs are
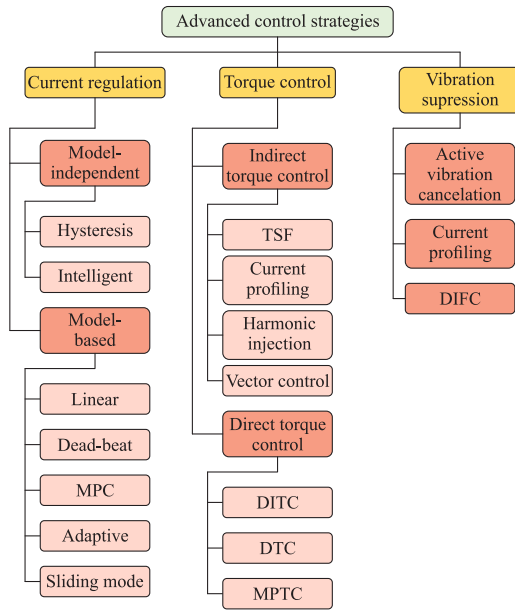
FIGURE 1. Classification of advanced control strategies for SRMs.

FIGURE 2. Cross section for a typical four-phase 8/6 SRM.

II. SRM FUNDAMENTALS

The switched reluctance motor presents a simple structure, composed of a double salient structure, with concentrated windings mounted on the stator slots. Thus, the machine presents a single source of excitation, on the stator. A typical cross section of a four-phase 8/6 SRM is shown in Fig. 2. In order to operate as a motor, the excitation of each phase of the machine must be done sequentially. For proper operation, a static converter and a closed loop control system are necessary [6]. This section presents the mathematical model of the SRM and a description of the asymmetric half-bridge converter, which is commonly used to drive the machine.

A. SRM MODEL

When neglecting the coupling between phases [31], the voltage across the phase terminals of a SRM is given by

$$v = Ri + \frac{d\phi}{dt}, \tag{1}$$

where ϕ is the flux linkage and R is the stator winding resistance. Magnetic saturation can be taken into account, with the flux linkage being a function of both current and rotor position, θ. Flux linkage, therefore, can be defined as:

$$\phi(\theta, i) = L(\theta, i)i(t). \tag{2}$$

Replacing (2) in (1) and calculating the flux linkage derivative, results

$$v = Ri + L(\theta, i)\frac{di}{dt} + i\frac{dL(\theta, i)}{dt}. \tag{3}$$

Expanding the derivative of the inductance in relation to time, results

$$\frac{dL(\theta, i)}{dt} = \frac{\partial L(\theta, i)}{\partial \theta}\frac{d\theta}{dt} + \frac{\partial L(\theta, i)}{\partial i}\frac{di}{dt}. \tag{4}$$

By replacing (4) in (3) and rearranging the terms yields

$$v = Ri + l(\theta, i)\frac{di}{dt} + e_b \tag{5}$$

where

$$l(\theta, i) = L(\theta, i) + i\frac{\partial L(\theta, i)}{\partial i} \tag{6}$$

$$e_b = i\omega_r \frac{\partial L(\theta, i)}{\partial \theta}. \tag{7}$$

characterized by a simple double salient construction, robustness, low production and maintenance costs and a rotor made of electrical steel [11]–[13]. Independent concentrated windings are mounted on stator slots, making the machine inherently fault tolerant. In addition to these features, the SRM is capable of operating over a wide range of speed and temperature [6]. These characteristics make the switched reluctance machine a viable option for several applications involving variable speed operation and hostile environments [14]–[19]. Moreover, SRMs are specially interesting for traction applications, being a growing topic of interest within the research community [20]–[26].

The switched reluctance machine, however, present some known drawbacks. The SRM is prone to high torque ripple, with the switched nature of the machine being the most contributing factor [27]. Moreover, when a phase is excited, large radial forces are generated, which deform the stator core and lead to increased vibrations and acoustic noise [28]. Such characteristics have been a deterrent to the mass adoption of this type of motor [29]. Lastly, when operating below base speed, current control is often employed. Due to the varying phase inductance and magnetic saturation effects, an adequate current controller is necessary in order to achieve proper current reference tracking. Poor tracking can lead to increased torque ripple as well as acoustic noise production [30].

Nonetheless, these characteristics should not prevent the wide use of SRMs. In order to overcome these challenges, many advanced control strategies have been proposed in literature. Thus, this paper focuses on presenting a review of the state-of-the-art solutions for the advanced control of SRMs, which encompasses current regulation strategies, torque control strategies and vibration suppression techniques. Fig. 1 shows a classification of the reviewed control strategies, which will be thoroughly analyzed in the following sections.
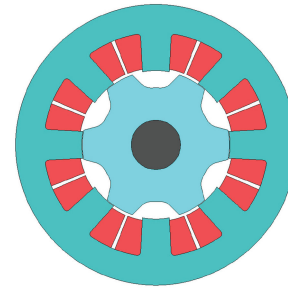
FIGURE 3. Tangential and radial forces generated in a SRM.

FIGURE 4. Torque ripple illustration for SRMs.

FIGURE 5. Four-phase asymmetric half-bridge converter.

The term $l(\theta, i)$, seen in (6), is known as the incremental inductance [32]–[34]. This term includes the effects of magnetic saturation, given it takes into consideration current, self-inductance $L(\theta, i)$ and the inductance variation caused by current. The term e_b, seen in (7), is the back-EMF of the machine. From (5), it can be seen that current regulation presents a challenge, given that $l(\theta, i)$ and e_b are dependent on both position and phase current, requiring the use of robust controllers.

The torque production in SRMs occurs due to the natural tendency of the rotor poles to seek alignment with the stator poles during excitation, thus, maximizing the inductance of the circuit. For an unsaturated SRM, the torque can be expressed as (8). The severe nonlinearity in the saturated SRM, however, prevents us to express the torque as a function of phase current and inductance.

$$T_e = \frac{1}{2}i^2\frac{dL\theta}{d\theta} \qquad (8)$$

By using the Maxwell stress tensor, the radial force, F_r, and tangential force, F_t, as shown in Fig. 3, can be calculated as:

$$F_r = \frac{1}{2\mu_0}\int_s (B_r^2 - B_t^2)ds$$

$$F_t = \frac{1}{\mu_0}\int_s B_r B_t ds \qquad (9)$$

where the B_r, B_t, μ_0, and ds represent the radial flux density, tangential flux density, vacuum permeability, and infinitesimal increment of the integral surface area. The tangential force acting on the rotor poles generates torque. Since the SRM is sequentially excited, the current and torque waveforms are inherent pulsed. Typical phase torque and total torque waveforms for an 8/6 SRM are shown in Fig. 4.

Two kinds of torque ripple can be observed, namely commutation torque ripple and high-frequency torque ripple. The commutation torque ripple results from the inherent pulsed toque waveforms, and normally it is the majority of the torque ripple. The high-frequency torque ripple is caused by switching actions during the current or torque regulation process and it is related to both the setup hardware and the machine parameters. Because the tangential force fluctuates and acts in the lateral direction of the stator pole, it also deforms the stator pole laterally and generates little noise. On the other hand, the radial force acts in the radial direction of the stator pole and
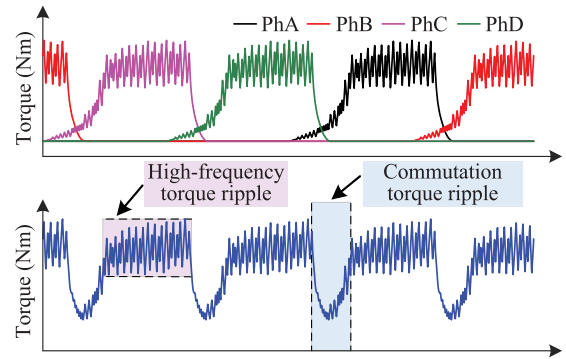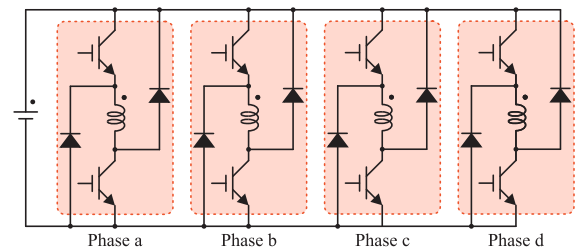
deforms the stator core, emitting noise. Due to the fact that B_r is normally much larger than B_t, the radial force is one order of magnitude larger than the tangential force. Therefore, the radial force is the main electromagnetic source to generate vibration and noise. Since the SRM has a unique salient rotor, it will also generate aerodynamic noise when the speed is high. To summarize, the torque ripple from the pulsed torque production mechanism and the vibration from the inherently large radial force pose as the two main issues for the wide application of SRMs.

B. ASYMMETRIC HALF-BRIDGE CONVERTER
A static converter is required for proper phase excitation and continuous operation of a SRM. The most commonly used topology is the asymmetric half-bridge (AHB) converter [35], shown in Fig. 5. The topology allows each phase to be controlled independently, where two switches and two diodes are used for each phase of the machine. The converter also presents versatility in the sense that it can be used to drive the machine as a motor or generator without major physical alterations.

Considering that each phase is excited individually, without overlapping, it is possible to analyze the switching states of the AHB converter separately, as presented in Fig. 6. The first switching state happens when both switches are closed and both diodes are blocked, as shown in Fig. 6(a). DC-link voltage is applied to the phase, causing current to rise while the switches remain closed, depicting the process of magnetization. Once the switches are opened, the energy stored in the winding causes the diodes to be forward biased, allowing
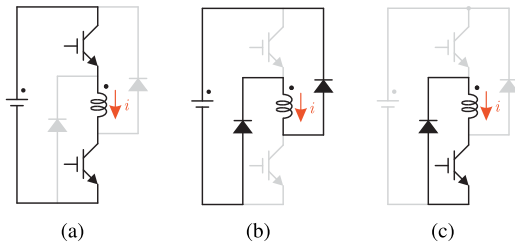
FIGURE 6. Asymmetric half-bridge converter switching states. (a) Magnetization. (b) Demagnetization. (c) Freewheeling.
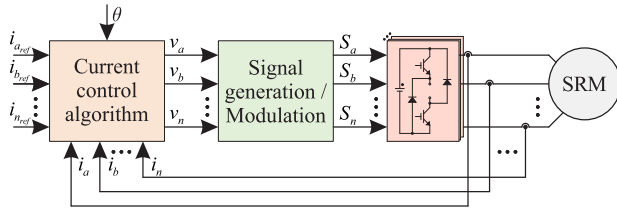

FIGURE 7. General block diagram for SRM current control.

FIGURE 8. General block diagram for SRM hysteresis current control.

FIGURE 9. General block diagram for SRM iterative learning current control.

current to flow through a new path. This starts the second switching state of the converter, as presented in Fig. 6(b). Negative DC-link voltage is applied to the phase, causing phase current to decrease and demagnetize the winding. The diodes remain in conduction until the switches are closed again or the phase current reaches zero. A third switching state can be used, where only one switch is kept closed and the other switch is opened, as presented in Fig. 6(c). This state is known as freewheeling, given that current flows only though the phase, a switch and a diode, with zero voltage being applied to the winding.

III. CURRENT REGULATION STRATEGIES

Conventionally, when a SRM operates below base speed, and assuming it has an adequate DC bus voltage, current control is imposed. The characteristics of the motor, such as torque ripple, are affected by the tracking capability and ripple of the current controller. Moreover, the SRM presents significant control challenges regarding its highly nonlinear behavior, due to varying phase inductance and magnetic saturation. Thus, high performance current control techniques have been investigated over the years. In this section, different current control strategies for SRMs are presented, highlighting their advantages and disadvantages. They are divided in model-independent and model-based strategies. A general SRM current control block diagram can be seen in Fig. 7.

A. MODEL-INDEPENDENT METHODS

1) CONVENTIONAL CURRENT CHOPPING CONTROL

Current chopping control is the most commonly applied method in SRM current control due to its independence on the model and fast dynamic response [36]. The strategy basically consists on the use of a hysteresis controller with a predetermined hysteresis band. Two different methods, named
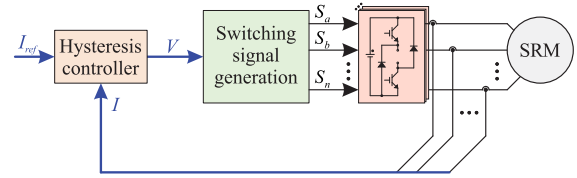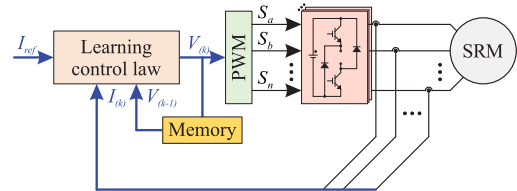
hard chopping and soft chopping, are characterized by the use of negative and zero voltage levels, respectively. The discrete number of possible duty cycles (1, 0 and -1) and the limited sampling frequency, significantly affect the reference tracking capability of this strategy. The resultant current ripple will be much more obvious at low-speed operation and for low inductance SRMs [6]. It should also be noted that the switching frequency varies in accordance with the control frequency and current hysteresis band, so the electromagnetic interface (EMI) should be carefully considered. Different methods have been reported in the literature to address the above-mentioned issues, while also seeking to improve current tracking capability. The block diagram of a hysteresis current control approach is presented in Fig. 8.

2) INTELLIGENT CONTROLLERS

As an alternative to the hysteresis controller, but still within the realm of model-independent strategies, intelligent control techniques have been investigated [37]–[42]. These strategies often rely on a learning mechanism in order to improve the controller's response. This can be performed online, with the controller being tuned by experimental measurements, or offline, based on sequential simulation results. The main advantages of such techniques are the ability to deal with highly nonlinear behavior, the ability to adapt over time to parametric changes and the fact they are model independent. In addition, these techniques may be implemented using PWM, resulting in a fixed switching frequency. The main drawbacks of these techniques are the relative slow learning process, the need for training data and significant computational complexity. An example block diagram of an iterative learning current controller is depicted in Fig. 9.

In [37] a two stage low torque ripple SRM control scheme is presented, where an iterative learning control (ILC) approach is used for both torque and current control. The authors further investigate the use of ILC for current regulation in [38],
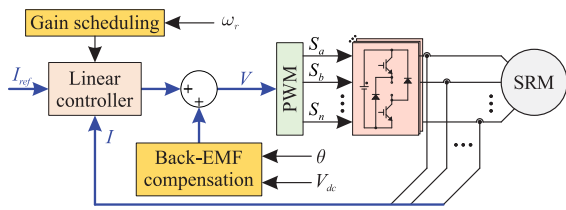
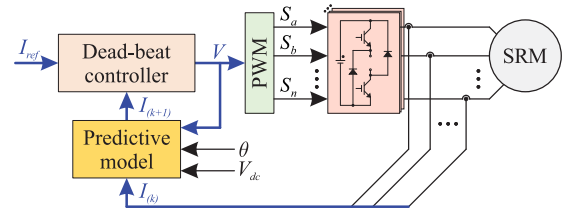**FIGURE 10.** General block diagram for SRM linear current controllers.

FIGURE 11. General block diagram for SRM dead-beat current controllers.

and propose a novel P-type feedback controller using an ILC block as a feedforward controller. The P-controller is tuned separately to achieve the best possible tracking performance and once the torque reference stabilizes, the ILC then further enhances current tracking. A Q-learning algorithm is used in [39] to provide adequate current tracking for SRMs. A scheduling mechanism is used in order to cope with the Q-learning algorithm limitations. Additional ILC based approaches are presented in [40], [41] and [42].

Other intelligent control techniques such as artificial neural networks (ANN) and fuzzy logic have been evaluated for torque control, torque sharing and current profiling of SRMs, as will be depicted in Section IV. However, it should be noted that, to the best of the authors knowledge, these techniques have not been considered in order to address the current regulation problem in SRMs.

B. MODEL-BASED METHODS

1) LINEAR CONTROLLERS

Linear controllers, such as the PI controller, are standard in industry applications. Several papers have investigated the use of such controllers for the current control of SRMs [43]–[57]. These strategies make use of mainly PI controllers to calculate a duty cycle for a PWM signal, based on the current tracking error. State feedback controllers have also been reported in [45] and [46], for example. Advantages such as a fixed switching frequency and lower current ripple when compared to hysteresis controllers are observed. Fig. 10 presents the block diagram of a possible linear control approach for SRM current control.

Due to the non-linear nature of the SRM, however, the design of linear controllers becomes a challenging task. To overcome this issue, some papers present a linearized modeling of SRMs for the design of closed-loop current controllers. Small-signal modeling is presented in [47] and [48], where a linear SRM model is derived for nominal operating conditions. In [49] a SRM is also linearized around its nominal operating point, allowing the gains of a PI controller to be tuned. In [50], a small-signal model is built initially, based on the inductance profile of the machine. Then, it is used for the design of a fixed gain PI controller.

The back-EMF of the machine is a disturbance that affects current control in SRMs, generally degrading the tracking capabilities of the controllers at medium and high speeds [50]. As a solution, some strategies make use of EMF compensation. In [51] and [52] back-EMF is estimated offline, from

flux-linkage data. The results are then stored in lookup tables, which are used in the digital implementation. In [53] online estimation is performed by means of a neural network, not requiring prior knowledge of the machine's characteristics. A back-EMF observer is used in [54] to achieve back-EMF cancellation. Even though ideal cancellation cannot be obtained, the technique allows the current changing rate to be increased. Moreover, the burden over the employed PI controller is lessened. A simple estimation method is presented in [50], where the back-EMF is calculated based on the SRM model. The resulting strategy is not computational or memory intensive. Another alternative for improving the performance of linear controllers is the use of gain scheduling strategies [55]–[57]. In [55] a variable gain PI controller is proposed, where the gains are adjusted as a function of both current and rotor position, ensuring better tracking performance. A parameter dependent controller using the linear parameter varying control approach is presented in [56]. A H_∞ control extension is chosen to design a gain scheduled current controller, by means of a polytopic representation. A convex optimization problem is built and, after solving linear matrix inequalities, the so-called self-scheduled controller is obtained by interpolation.

2) DEAD-BEAT CURRENT CONTROLLER

Alternative control techniques, such as dead-beat controllers, have also been investigated for the current control of SRMs. Dead-beat control makes use of a predictive model as a means to determine which voltage value should be applied in order to produce zero tracking error in one digital time step. This technique presents as a main advantage a fast dynamic response. Moreover, dead-beat controllers are typically implemented with PWM, ensuring a fixed switching frequency. A known disadvantage of dead-beat controllers is the fact they rely on an accurate model and large gains. This means that model uncertainties and noise in measurements may significantly degrade the performance of the dead-beat controller, which can even lead to stability issues. Several dead-beat current control approaches have been proposed for SRMs [36], [58]–[64]. An example block diagram for a dead-beat current controller is presented in Fig. 11.

In [58] and [59] a dead-beat predictive current controller is proposed. The proposal is capable of predicting the necessary duty cycle for the PWM pulses for any given reference current at every digital time step over the entire speed range. Similar proposals are also described in [60] and [61], with the latter
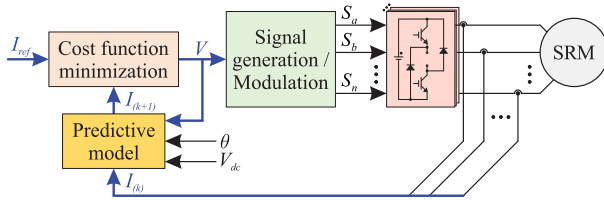
FIGURE 12. General block diagram for SRM model predictive current controllers.

FIGURE 13. General block diagram for SRM adaptive current controllers.

being applied to mutually coupled SRMs. A flux-based and a back-EMF-based approach are presented, where both make use of machine data, stored in the form of lookup tables. A dead-beat PWM controller is designed in [36]. The proposal makes use of the SRM model in order to achieve fast response and accurate reference current tracking. As a means to deal with the SRM's nonlinear behavior and correct the model mismatch, a gain observer is introduced. In [63] a predictive dead-beat current controller is used in a current injection scheme for SRM characterization, avoiding traditional rotor-locking strategies. A deadbeat current control strategy with active thermal management is proposed in [62]. The controller is used as an alternative to hysteresis. This allows for lower switching frequencies, while still maintaining suitable performance. The frequency is dynamically adjusted based on the IGBT temperature measurements, avoiding damage by overheating.

3) MODEL PREDICTIVE CURRENT CONTROLLER

Another class of predictive current controllers used for SRM current control are the model predictive controllers (MPC). These technique is characterized by the minimization of a cost function as a means to determine the control output. It can be divided in two different approaches: continuous control set (CCS), where a modulator determines the switching states based on the continuous output of the predictive controller, and finite control set (FCS), where the limited number of switching states are considered for solving the optimization problem [65]. MPC methods present as advantages the use of an optimal control law and the possibility of including nonlinearities in the predictive model. On the other hand, MPC often presents increased computational effort for systems with increased number of switching states. Moreover, the performance of the controller is affected by the quality of the model. Lastly, in the case of FCS-MPC, no modulator is used. This results in a variable switching frequency, which is not desirable for SRM current control applications [66]. In this context, multiple contributions have been made regarding MPC applied to SRM current control [67]–[73]. A model predictive current control structure for SRMs is depicted in Fig. 12.

A model predictive current controller (MPCC) for SRMs is proposed in [68]. The proposal makes use of state estimators and model identification, in the form of an online inductance estimator, as a means to improve performance.
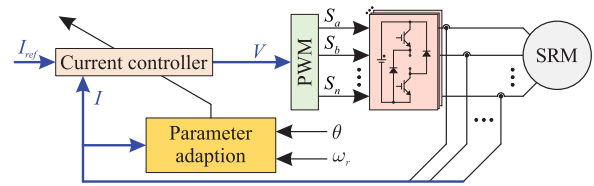
Other advantages, such as delay compensation and a fixed switching frequency, are also observed. A similar approach is presented in [69], where an unconstrained MPCC is combined with an inductance auto-calibration mechanism, resulting in a stochastic MPCC with adaptive model calibration. A MPCC making use of a high accuracy lookup table (LUT) based on a semi-numerical machine model is described in [70]. In [71] a virtual-flux FCS-MPCC for SRMs is proposed. The strategy uses flux-linkage tracking in order to indirectly control phase currents. A cost function is used to determine the switching signals that deliver minimum error and, in order to reduce commutations and computational complexity, a state graph for switching states limitation is proposed.

The use of MPCC has also been observed in other types of SRMs. In [72] an adaptive model predictive current controller for a double stator SRM (DSSRM) is proposed. The adaptive estimator is used as a way to cope with the time varying inductances of the DSSRM. In [73] FCS-MPCC is applied to the current control of a mutually coupled SRM (MCSRM), as previous proposals for regular SRMs with AHB converters cannot be directly applied to MCSRM.

4) ADAPTIVE CURRENT CONTROLLER

Another alternative to deal with the highly nonlinear behavior of SRMs is to dynamically adjust the controller gains. This allows the controller to be tuned online based on speed or load, for example, improving the dynamic responses and system stability. Such techniques also present as an advantage a fixed switching frequency, given they are implemented with PWM. It should be noted that adaptive controllers present cumbersome calculations, resulting in a more complex controller when compared to linear approaches, for example. Some adaptive current control strategies have been proposed in literature [49], [74], [75]. The block diagram of an adaptive current controller for SRMs is presented in Fig. 13.

In [74] a model reference adaptive current controller is proposed. In this approach, a model with the desired characteristics, named reference model, is chosen. Such model is run in parallel with the closed loop system, where a gain adaptation mechanism is responsible for eliminating the difference between both outputs. An additional advantage of the proposal is the fact no SRM parameter lookup tables are required. A multi-loop self-tuning adaptive PI controller is presented in [49]. Firstly, a linearized model of the machine is considered. Then, the gains of the controllers are updated online as a function of the tracking errors, resulting in
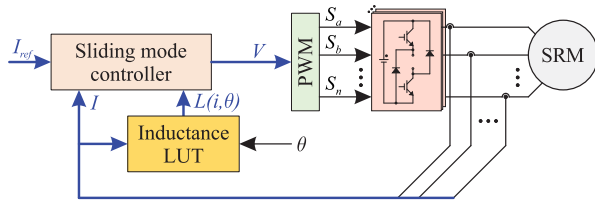
FIGURE 14. General block diagram for SRM sliding mode current controllers.

superior transient responses when compared to a fixed gain PI controller. Moreover, the controller presents a simple structure when compared to other nonlinear strategies.

An adaptive digital PWM current controller is described in [75]. Online gain adaptation is employed to deal with the model mismatch, ensuring both suitable dynamic responses and robustness to the algorithm. It takes full advantage of the SRM model information. Discrete-time analysis is presented, along with an improved sampling method to avoid the inherent PWM delay. The relationship of the proposal and other controllers is evaluated, showing it as an improved version of PI and dead-beat controllers.

5) SLIDING MODE CURRENT CONTROLLER
Sliding mode algorithms have also been proposed as an alternative to address current control in SRM drives [76]–[85]. The technique is of interest mainly due to its robustness, necessary to deal with the nonlinear behavior of the machine. Moreover, due to PWM implementation, these techniques present a fixed switching frequency. Fig. 14 presents the block diagram of a possible sliding mode control approach for SRM current control.

In [76] a sliding mode controller is presented. The proposal is further developed in [77], where a carrierless structure is used, with a state machine being responsible for uniform converter switching. The controllers are inherently designed for digital implementation given that they are based on the sliding mode control theory. In [78] an adaptive sliding mode current controller is proposed. The design is carried out using a simple linear model, while the non-linear characteristics are considered as disturbances and uncertainties. Gain adaptation is employed as a means to improve the dynamic response and reduce chattering. An additional adaptive sliding mode strategy is presented in [79]. A sliding mode-PI control approach is presented in [80]. The combination of both techniques allows for suitable reference tracking combined with robustness. An integral sliding mode current controller with constant switching frequency is proposed in [81]. The controller is designed considering a state space model with self and mutual inductances, where the stability analysis is presented for both known and bounded uncertain parameters situations. The proposal is evaluated for mutually coupled switched reluctance motors in [82] and [83], with the SRM being driven by an AHB and a three-phase voltage source inverter, respectively.

In practical applications, conventional sliding mode control strategies present chattering as a major drawback. Chattering is often referred to as a phenomenon of finite frequency and amplitude oscillations, resulting from sliding mode control. It is undesirable given it can lead to lower control accuracy and, on the SRM application, increased current ripple. Higher-order sliding modes are able to overcome this issue without significant compromises while maintaining a similar level of complexity. A second order sliding mode (SOSM) current controller is proposed in [84], with gain design being carried out through successive tests. Experimental results show the robust characteristics of the controller to phase inductance variations. More recently, in [85] a SOSM controller is proposed. A comparative study is presented, with the SOSM controller presenting superior performance when compared to a traditional sliding mode approach, specially regarding the chattering phenomena.

C. COMPARISON OF THE CURRENT CONTROL STRATEGIES
The comparison of SRM current control strategies reported in literature is presented in Table 1. The previously discussed techniques are compared in terms of advantages, disadvantages, the use of model information (i.e. lookup tables), computational complexity and if fixed switching frequency is observed.

The traditional hysteresis controller is a simple model independent approach, however, it presents variable switching frequency and may present increased current ripple. Intelligent control is able to deal with the SRM nonlinearities, but requires data and extensive training. Linear control approaches are industry standard, but do not present the required robustness, often requiring gain adaptation or back-EMF compensation. Dead-beat controllers present predictive capabilities and fast dynamic response, however, are sensitive to model uncertainties and noisy measurements. In this sense, MPC presents an optimal control law and takes nonlinearities into consideration, at the cost of requiring cumbersome calculations. Adaptive techniques are robust and capable of online adaptation but often present complex calculations and a complex structure. Lastly, sliding mode approaches are capable of fast dynamic responses with a theoretical certificate of robustness. Chattering is a known drawback of the technique, which can be circumvented by adequate gain design, gain adaptation or the use of higher order sliding modes.

IV. TORQUE CONTROL STRATEGIES
Although the double salient structure brings merits to SRMs, such as low manufacturing cost and ruggedness, it also brings some drawbacks: (1) the phase torque is pulsed and (2) there is no reference transformation to eliminate the position from its voltage and torque expression [86]. Hence, the well-known vector control method, used in AC machines, cannot be directly transferred to the SRM. This poses difficulties with regards to the torque control for SRMs. For decades, researchers have been focusing on this field and numerous methods are proposed to regulate the output torque. These methods can

TABLE 1. Summary and Comparison of the SRM Current Control Strategies

| Technique	Advantages	Disadvantages	Model information	Computational complexity	Switching frequency	References
Hysteresis	Simplicity, robustness, fast dynamic response	Variable switching frequency, higher current ripple	No	Low	Variable	[6], [36]
Intelligent	Over time adaptation, good for non-linear problems	Slow learning process, need for training data	No	Medium	Variable/Fixed	[37]–[42]
Linear	Industry standard, simplicity	Not robust, poor fixed gain performance	No/Yes	Low	Fixed	[43]–[57]
Dead-beat	Fast dynamic response, predictive	Sensitive to model uncertainties and noise	Yes	Medium	Fixed	[36], [58]–[64]
MPC	Optimal control law, consideration of nonlinearities	Cumbersome calculations, no modulator (FCS), model dependent	No/Yes	High	Variable/Fixed	[67]–[73]
Adaptive	Robustness, online adaptation	Cumbersome calculations, complex structure	No/Yes	High	Fixed	[49], [74], [75]
Sliding mode	Robustness, fast dynamic response	Chattering	No/Yes	Medium	Fixed	[76]–[85]
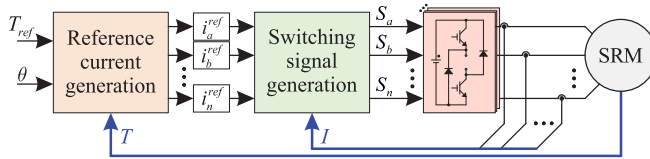
FIGURE 15. General block diagram for indirect torque control.

be categorized as indirect and direct methods, as depicted in Fig. 1, based on the control objectives observed in the control loop.

A. INDIRECT METHOD

Since current is related with electromagnetic torque in SRMs, indirect control methods regulate the output torque by controlling phase current. Fig. 15 describes the general block diagram for an indirect torque control structure. The reference current for each phase is firstly generated according to the torque command, T_{ref}, position information, θ, and reference current generation algorithm. The feedback instantaneous torque might also be used in this process. Then, the corresponding switching signals are generated with the aid of the actual phase current and later applied to the inverter so the phase current attempts to track its reference value. The torque control performance relies on the reference current generation algorithm and the switching signal generation method. Among the existing literature, the indirect control methods can be roughly divided in torque sharing functions (TSF), current profiling techniques, harmonic current injection and vector control strategies.

1) TORQUE SHARING FUNCTIONS

Due to the pulsed nature of the output phase torque in SRMs, the total torque to be produced needs to be shared between the active phases in the commutation region. The use of

TSFs works in a rather straightforward way, where appropriate torque references are generated for each phase. Then, an important nonlinear function $i(T, \theta)$ is utilized to convert the torque reference to the corresponding current reference. As torque is a highly nonlinear function of current and position, the torque control performance is significantly affected by the TSF used [6].

TSF method can be traced back to [86], where the total torque is distributed to each phase in a pattern of a mathematical function, with an exponential TSF being presented in order to deliver the constant total torque. A more general expression for the TSF method can be described as (10) and (11),

$$T_{total} = T_{ref} \times f_T(\theta) \tag{10}$$

$$f_T(\theta) = \sum_1^n f_k(\theta) = 1 \tag{11}$$

where T_{total}, T_{ref}, $f_T(\theta)$, and $f_k(\theta)$ are total shaft torque, reference torque, sum of the distribution function and phase distribution function, respectively. Numerous kinds of the $f_T(\theta)$ can be found in the literature.

According to the torque distribution scheme, TSFs can be categorized as analytical TSFs, dynamic allocation TSFs and numerically optimized TSFs. The analytical-expression-based reference torque distribution function is the most straightforward allocation scheme, which uses a simple analytical expressions to represent the phase reference torque. The linear [87], sinusoidal [43], cubic [88] and exponential [86] TSF functions are most commonly employed in literature. A cubic TSF function is shown in Fig. 16, where the θ_{on}, θ_{ov}, and θ_{off} indicate turn-on angle, overlap angle, and turn-off angle, respectively. These parameters have great effects on the torque control performance for the TSF method. In [89], a genetic algorithm (GA) is used to optimize the turn-on angle and overlap angle for the four previously mentioned functions. Moreover, the rate-of-change of the flux-linkage and
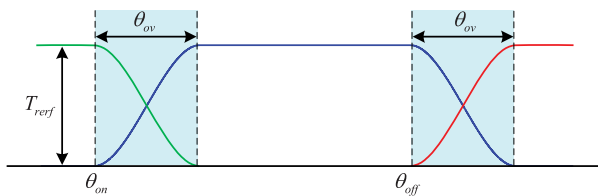
FIGURE 16. Example waveforms of a torque sharing function based strategy.

root mean square (RMS) value of the phase current were also compared. In [90] a family of reference current waveforms is analytically derived, with minimized p-norm, based on an inverse torque model. The linear SRM model was used to derive the current reference in [91], and the nonlinear torque features were included based on a nonlinear modulation factor.

Due to the limited current changing rate of the drive system, the reference current derived from the above analytical reference torque might not be tracked, especially at high speed and heavy load conditions [6]. In this case, the torque control performance is deteriorated. To address this issue, the dynamic allocation scheme distributes the phase reference torque in a way that considers the output torque capability of the incoming and outgoing phases. In [92], the pre-assigned linear torque reference is readjusted based on the maximum output torque capability of the machine. The special position in which the incoming phase is able to provide the reference torque divides the commutation region into two subregions. In different subregions, the phase with higher torque per ampere ratio was reassigned a higher reference torque [93]. In [94]–[96], the torque tracking error is estimated with the instantaneous torque feedback. The error is compensated with the phase with the higher torque output capability during the commutation period, while [97] utilizes a fuzzy-logic controller to adjust the torque reference. In [98], the reference torque is adjusted in such a way to demagnetize the outgoing phase as soon as possible, aiming to smooth out the output torque. The commutation region is divided into two subregions considering the absolute rate of change of the flux-linkage for the incoming and outgoing phase in [99]. The developed feed forward PI compensator helps to improve the torque control performance at high speed operating conditions. In [37], [100], [101], intelligent control strategies, such as ILC and neural networks, are adopted to correct the initial reference current derived from the simple analytical TSF with the instantaneous torque feedback.

Apart from torque ripple reduction, other metrics such as average torque, copper losses, and torque-ripple-free speed are also vital criteria when evaluating the performance of a drive. This problem is suitable for a standard numerical optimization procedure, where the copper losses might be the objective function, the constant torque requirement is the equality constraint, and other conditions such as the current limitation form the inequality constraints, for example. Taking advantages of global numerical optimization algorithms, such as GA, the reference current which meets the requirements at

different operating conditions can be obtained. In [102] the optimal reference current is determined aiming to minimize current RMS value while considering bus voltage limitations. In [103], optimized TSFs are extended to negative torque production, giving enough time to increase or decrease current, allowing for good performance at high speed operation. The current profiles are given by a series of B-spline functions, significantly reducing memory requirements. Moreover, copper losses and voltage limitations are also considered as secondary objectives in the optimization procedure. A new offline optimized torque sharing function is presented [104], where the squared current and its derivative were optimized through the method of Lagrange multipliers. A multi-objective GA algorithm is employed to find a suitable parameter that balances the compromise between copper losses and torque ripple reduction performance, while also considering current tracking capability [105]. A new torque sharing function is proposed in [106], aiming not only to improve torque control performance at high speed and heavy load but also reduce the current tracking error.

The three categories of TSF, described previously, are summarized in Fig. 17, where the expression, references, merits and drawbacks of each approach are presented.

2) CURRENT PROFILING TECHNIQUE

Unlike the TSF method, which distributes the reference torque first, the current profiling technique is another effective indirect approach which directly determines the reference current, without making use of the $i(T, \theta)$ lookup table. Normally, the current profiling method starts from a simple reference current and requires fine-tuning to reach the final reference current with good torque control performance. The phase current was arranged to rise and fall linearly during the commutation region in [107]. An initial reference current with trapezoidal shape was utilized and then tuned twice with instantaneous torque feedback to obtain the final reference current profile in [108]. The work was extended in [109] to a four quadrant operation, and further enhanced in [70] by considering the rate of current variation, improving high-speed performance. The work of [110] analytically derived the reference current based on the unsaturated SRM to not only reduce the torque ripple but also suppress the bus current ripple. The rotor shape design is also optimized with the intent of helping to minimize copper losses. It should be noted, however, that this method only works for unsaturated SRMs. In [111], the reference current is expressed by means of a Fourier series and a numerical optimization is used in order to determine the optimal coefficient. A common rectangular reference current is shaped with the aid of the negative part of the bus current and commutation shifting scheme in [112], with the intent of reducing torque ripple. Additional current profiling techniques which employ intelligent control can be found in [113]–[115].

3) HARMONIC CURRENT INJECTION

Since the current and inductance profiles are periodical in steady state, it is beneficial to analyze the effects of each
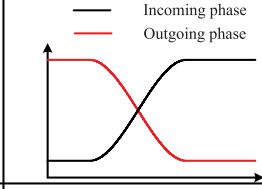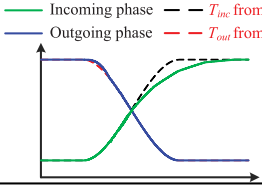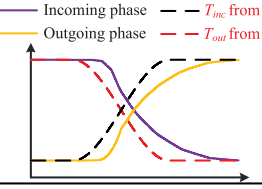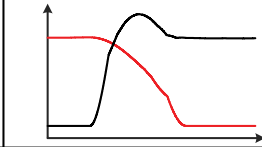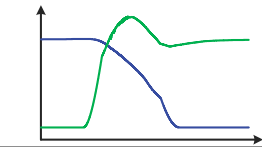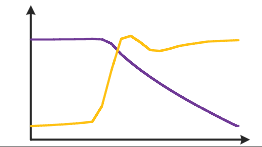
TSF method	Analytical function (AF)	Dynamic allocation (DA)	Numerical optimization (NO)
Possible expression	$\begin{cases} f_{inc} = g(\theta) \\ f_{out} = 1 - g(\theta) \end{cases}$	$\begin{cases} f_{inc} = g(\theta) + \Delta f_{inc} \\ f_{out} = 1 - g(\theta) + \Delta f_{out} \end{cases}$	$\begin{cases} minimize \quad f(x) \\ subject\ to \quad T_{inc} + T_{out} = T_{cmd} \\ inequality\ constraints \end{cases}$
Torque reference			
Current reference			
Merits	(1) Easy to implement (2) Good performance at low speed range	(1) Good torque control performance at wide speed range	(1) Good performance at wide speed range including second objectives
Drawbacks	(1) The current is hard to track at high speed	(1) Other metrics, such as copper loss, are not considered	(1) Computationally intensive (2) Large amount of data to be stored

FIGURE 17. Illustration of the TSF method. (Note 1: f_{inc}, f_{out}, T_{inc}, and T_{out} represent the incoming phase torque distribution function, outgoing phase torque distribution function, incoming phase reference torque, and outgoing phase reference torque. Note 2: The dashed black and red lines in the last two columns represent the torque reference from the analytical TSF).
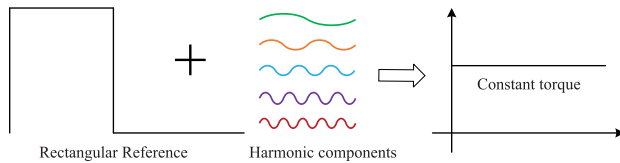

FIGURE 18. General block diagram for the harmonic current injection method.

current harmonic component on the torque ripple and average torque. As reported in [116] and [117], the average torque is mainly contributed by the DC, first order and second order harmonics, while the fourth and fifth harmonics have a more significant affect on torque ripple. In this case, it is possible to improve the output torque quality by actively and selectively injecting current harmonics, as shown in Fig. 18.

The injected current I_{inj} can be described as (12) [118],

$$I_{inj} = \sum_{1}^{n} I_n \cos(nN_r\theta + \varphi_n) \tag{12}$$

where I_n and φ_n indicate the magnitude and phase for the n-th order injected current, N_r represents the rotor pole numbers. In [118], the first five current harmonics with optimized amplitude and phase are superimposed on the rectangular current reference to improve the torque control performance in the low speed region. The method is extended to the high speed range in [119], where optimized current harmonics are determined online though the use of the simplex method. Five kinds of current references based on the half-sine waveforms are presented in [120], seeking to suppress torque ripple. Proper current harmonics are determined though numerical

optimization in order to reduce the torque ripple and radial force ripple simultaneously in [121] and [122]. A segmented harmonic current was optimized online through fuzzy logic to suppress torque ripple in [123].

4) VECTOR CONTROL

With the advent of the Park's transformation and the widespread use of vector control strategies, the torque control performance of AC machines was greatly enhanced. Unfortunately, in the early development of SRM control strategies, [86] and [124] proved that there is no such transformation to decouple the position from the flux-linkage and torque for SRMs even in the linear case. Nevertheless, for decades, researchers sought approaches to control SRMs using vector control strategies, with the intent to improve torque control performance.

According to the torque expression for the unsaturated SRM, [125], [126] constructed two rotating complex vectors, namely complex derivative of inductance vector $\overline{\dfrac{dL(\theta)}{d\theta}}$ and complex squared current vector $\overline{I(\theta)^2}$, as expressed in (13) and (14):

$$\overline{\frac{dL(\theta)}{d\theta}} = \sum_{N} \frac{dL(\theta)}{d\theta} e^{j(k-1)\frac{2\pi}{N}} \tag{13}$$

$$\overline{I(\theta)^2} = \sum_{N} I(\theta)^2 e^{j(k-1)\frac{2\pi}{N}} \tag{14}$$

where N indicate the number of phases for the employed SRM. A closed form of the torque-ripple-free phase current is derived for the unsaturated SRM. However, iterative calculation is required in the reference current generation for the
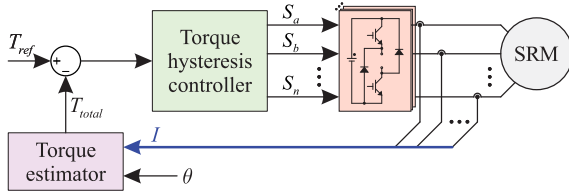
FIGURE 19. General block diagram for DITC.

FIGURE 20. General block diagram for DTC.

saturated SRM. In [127], [128], the authors directly map a synchronous reluctance machine to the SRM, by maintaining equal torque. From the perspective of control variables, the SRM is controlled in a vector torque control like method. However, note that phase current is not sinusoidal for both of the above mentioned methods.

In [129] is presented that the bipolar sinusoidal current excitation reduces the torque ripple but delivers lower average torque compared to the unipolar rectangular current excitation. Since the majority of the torque is generated by the DC and first two harmonics [116], [117], the DC plus first harmonic current excitation, as shown in (15), for the vector control method are intensively studied.

$$i_N = I_0 + I_1 \cos\left(N_r\theta + (N-1)\frac{2}{3}\pi + \varphi_1\right) \quad (15)$$

It is detailed in [130] that in SRM drives with unipolar current excitation, the DC component virtually generates the rotor flux and that the AC component generates the rotating stator field. A vector controller was developed based on the average value of the first order inductance and the relationship between the q-axis current and torque was derived, but only for the unsaturated SRM. An improved current controller for this vector control strategy is presented in [131]. The vector controller was further studied in [132] and [133], from the perspective of space vector modulation and variable q-axis current control. In [134], an alternative explanation of the DC plus first order current excitation is presented, based on the flux modulation principle. Although the speed of the SRM can be controller in the dq frame, the exact torque expression is not derived.

B. DIRECT METHOD

Directly regulating torque with the torque feedback and manipulating the power transistors is a more straightforward way to control the output torque compared to doing it indirectly. According to the existing literature, the direct method can be categorized as: direct instantaneous torque control (DITC), direct torque control (DTC) and model predictive torque control (MPTC).

1) DIRECT INSTANTANEOUS TORQUE CONTROL

Direct instantaneous torque control method was first presented in [135], [136], with Fig. 19 describing the general block diagram of this method. The key components in the DITC method are the toque estimator and torque hysteresis controller. With the instantaneous total torque calculated from the
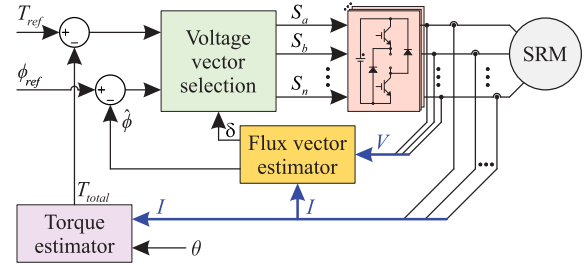
toque estimator and knowing the reference torque, the torque tracking error can be easily obtained. Then, the torque hysteresis controller generates the appropriate switching signals based on the estimated torque error and position information.

In [135], [136] it is validated that the DITC method could deliver smooth torque up to the rated speed with the appropriate conduction angles in the motoring mode. The work is extended in [137], developing the method to four quadrant operation and further reducing the torque ripple through the adoption of a predictive step and the use of PWM control in [138]. The turn-on and turn-off angles are optimized online in [139] to achieve better torque ripple reduction. Other performance enhancements, such as minimum torque ripple point tracking [139], [140], efficiency improvements [141]–[145], lower torque ripple through the use of multi-level inverters [146], [147], torque-ripple-free speed range extension [148], [149], and lower cost algorithms [150] were developed in recent years.

2) DIRECT TORQUE CONTROL

It is well-known that good torque control performance can be achieved by adopting the DTC method, as it was first presented for induction machines (IM). Thus, researchers tried to apply this control strategy to SRMs, with the intent to reduce torque ripple. Similar to the DTC method in IMs, [151], first the torque expression is derived as a means to build the link between the instantaneous torque and the flux-linkage variation, as shown in (16):

$$T \approx i\frac{\partial\phi}{\partial\theta}\bigg|_{i=constant} \quad (16)$$

This approximate formula indicates that the instantaneous torque can be regulated by accelerating and decelerating the spatial combined flux-linkage vector under the constant current assumption. Based on this concept, the general block diagram for the DTC method for SRMs can be depicted in Fig. 20.

The toque error, flux-linkage error, and flux-linkage vector sector information are responsible for deciding the appropriate voltage vector which could keep the torque and flux-linkage within a hysteresis band. The work of [152] points out several key concepts when implementing the DTC method, including the flux-linkage reference value in different operating conditions and the difference between the flux-linkage
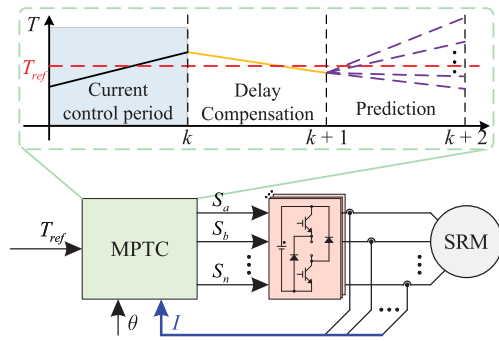
FIGURE 21. General block diagram for MPTC.

vector position and actual rotor position. Improved voltage vectors are used to enhance the torque control performance in [153]–[156]. The speed-dependent flux-linkage reference was presented in [157] to reduce the phase current RMS value. A dead-beat DTC is developed in [158] to further reduce the torque ripple. The function of the flux-linkage loop was explained in [159] in detail, and the authors suggest to remove this loop since the constant flux-linkage does not means constant torque in SRMs. The torque per ampere ratio is significantly enhanced by eliminating the negative torque. In [160], the speed loop PI regulator is replaced by a sliding mode controller along with a disturbance observer in order to improve the dynamic performance of the DTC method.

3) MODEL PREDICTIVE TORQUE CONTROL

The MPTC method regulates the electromagnetic torque by considering the possible future states for all available voltage values. A typical control block diagram for the finite-set MPTC method with one control period delay compensation and one sample prediction horizon is shown in Fig. 21.

According to the sampled phase current, position, and the applied voltage vector calculated at the previous control period, the phase current and total toque at future control periods can be estimated based on the employed SRM model. Then, a scalar cost function is adopted to evaluate the control performance under different candidate voltage vectors and the one that presents minimal cost is selected to be applied to the SRM in the next control period. An example of one commonly utilized cost function is expressed as (17):

$$J = (T_{ref} - T_{total}(k+2))^2 + \omega_1 \sum (i(k+2))^2$$
$$+ \omega_2 \sum (S(k+1) - S(k))^2 + g(i(k+2))$$
$$g(i(k)) = \begin{cases} \infty, & \text{if } i(k) \geq i_{MAX} \\ 0, & \text{if } i(k) < i_{MAX} \end{cases} \quad (17)$$

where ω_1 and ω_2 are the weighting factors [161], $S(k+1)$ and $S(k)$ are the switching states, and T_{total} is the sum of the phase torque. It is observed that the total torque error, copper losses, switching losses and maximum current limitations, for example, can all be included in the cost function. By carefully tuning the weighting factors, the drive control performance

regarding torque ripple, copper losses and average switching frequency can be simultaneously improved, which is one of the merits of MPTC.

The MPTC method was first applied to SRMs in [161], based on a versatile analytical SRM model. It was later extended in the work of [162] with virtual discrete voltage vectors to further reduce torque ripple. In [163] and [164] model predictive control is employed as an inner current control loop, allowing the phase torque to track the pre-assigned reference with minimal error. The Fourier expansion and exponential function based analytical SRM model along with improved switching tables are used in [165] to implement the MPTC. Large torque ripple and low torque per ampere ratio issues related to the significant negative torque in high speed operating conditions were explained in [166] and improved by the use of an adaptive turn-off angle.

C. COMPARISON OF THE TORQUE CONTROL METHODS

All the torque control methods presented above can significantly reduce the torque ripple to a certain extent but might differ in the torque-ripple-free speed. In order to comprehensively show the difference of the presented strategies, a list of some key aspects of each method is presented in Table 2.

In general, the analytical TSF method possesses simplicity and delivers smooth torque in the low speed region. However, its torque control performance at medium and high speed region is degraded due to the low reference current trackability. The dynamic allocation TSFs improves its torque control performance at medium and high speed region but might sacrifice other performance aspects, such as copper losses and overall efficiency. To simultaneously enhance the performance on the torque control and other aspects, like copper losses, the turn-on and overlap angles need to be optimized, either online or off-line, increasing complexity. As for the numerically optimized TSFs, although they may take substantial computational effort to obtain the reference current waveforms and require large amounts of memory on implementation, this method not only can generate smooth torque at high speeds but also exhibits the highest flexibility level when considering the second objective of the optimization, which can be copper losses and average torque, for example. Current profiling and harmonic injection can deliver smooth torque to a certain speed region, but show limited performance when it comes to a secondary objective, since the reference current for both methods has to meet a specific shape. The vector control method normally shows good torque control performance at light load conditions, but suffers at heavy load conditions due to the severe saturation in the SRM. The above methods are all indirect, thus requiring the use of a current control loop and making the torque control performance dependant on the current controller's tracking capability.

On the other hand, the DITC, DTC and MPC are direct methods, where the torque control performance is directly related with the control method itself. With proper choice of the switching angles, the DITC method can deliver smooth torque up to rated speed and the copper losses can be reduced

TABLE 2. Summary and Comparison of the SRM Torque Control Strategies

Method	Implementation complexity	Torque-ripple-free speed	Computational burden on MCU	Consumed storage space	Current loop	Switching angles
Analytical TSF	Simple	Low	Low	Low	Yes	Yes
Dynamic allocation TSF	Simple	High	Low/Medium	Low	Yes	Yes
Numerical optimization TSF	Complex	High	Low	High	Yes	No
Current profiling	Complex	High	Low	High	Yes	No
Harmonic injection	Medium	Medium	Medium	Low	Yes	Yes
Vector control	Medium	Low/Medium	Medium	Low	Yes	Yes
DITC	Simple	High	Low	Low	No	Yes
DTC	Medium	Low/Medium	Low/Medium	Low	No	No
MPTC	Simple	Medium	High	Medium	No	No

(Note: MCU Stands for Microcontroller Unit, and Switching Angles Refers to the Turn-On and Turn-Off Angles)
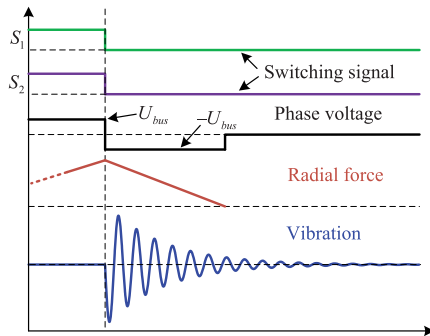

FIGURE 22. Vibration generation process for the SRM under single pulse voltage control.
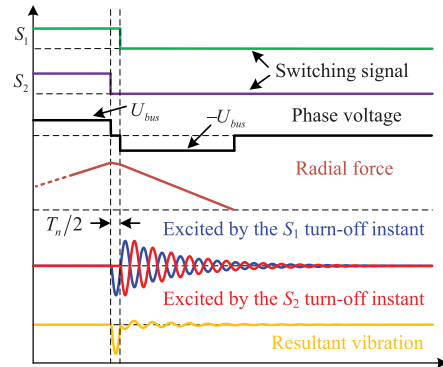

FIGURE 23. Vibration reduction by the two-stage commutation method.

by optimizing the commutation interval. Due to the extra flux-linkage loop in the DTC method, the torque-ripple-free speed and efficiency of the technique are limited. The MPTC method possesses the advantage of optimizing different objectives through a simple scalar cost function and does not require the switching angles to be varied at different operating conditions. However, the heavy computational burden and significant negative torque at the high speed region are the main drawbacks for this method.

V. VIBRATION SUPPRESSION STRATEGIES

Due to the nature of the double salient structure and the minimum reluctance working principle of SRMs, radial force is unavoidable when a phase winding is energized. Typically, the radial force is one order of magnitude larger the tangential force, which makes the stator deform as a result. Then, the generated vibration emits acoustic noise to the surrounding environment. If the harmonics of the radial force coincides with the natural frequency of the SRM, loud acoustic noise will be perceived. To mitigate this issue, researches have proposed many effective methods to reduce vibrations and acoustic noise, which could be roughly divided as active vibration cancellation method, current profiling and direct instantaneous force control (DIFC).

A. ACTIVE VIBRATION CANCELLATION

The vibration generation process for the SRM under single pulse voltage control is depicted in Fig. 22. During the turn-off instant, the gradient of the radial force is suddenly changed,

which effectively equates to the point of impact of a hammer on the stator core [167], so the damped vibration is generated at the natural frequency of the stator. The authors in [168] proposed the two-stage commutation process, which deliberately introduces another vibration $T_n/2$ after the first commutation instant to actively cancel the vibration generated by the first radial force gradient variation instant, as shown in Fig. 23. It is noted that $T_n/2$ is half the period of the dominant vibration mode. To ensure the effectiveness of the two-stage commutation method, the voltage before and after the turn-off instant should be equal and the introduced zero-voltage period should be close to $T_n/2$.

Because the current chopping method is normally applied in the low speed region, the effective voltage applied before the turn-off instant is lower than the bus voltage. To improve the noise reduction at the above case, [169] modified the demagnetization period with two voltage steps instead of directly applying negative bus voltage. In [167] is presented an alternative form of the two-stage commutation method, named three-stage commutation, which can be employed when the converter cannot provide the freewheeling stage. The work of [170] employs variable bus voltage, provided by a front-end circuit, to force the phase current to be controlled under switching angle control at all operating conditions, enabling the two-stage commutation method to be effectively applied at all times. The switching instant in [171] is arranged in a way to at least partially cancel the vibration generated by the previous switching instant, reducing noise while in current
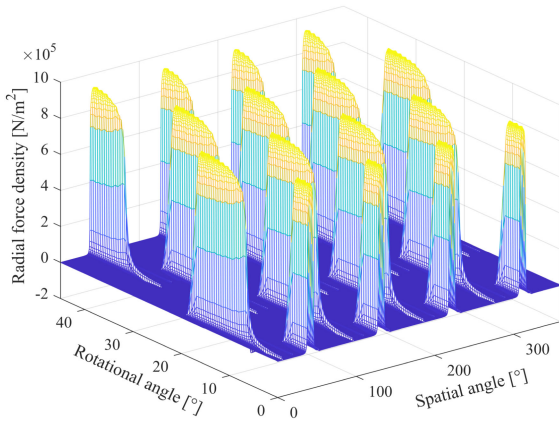
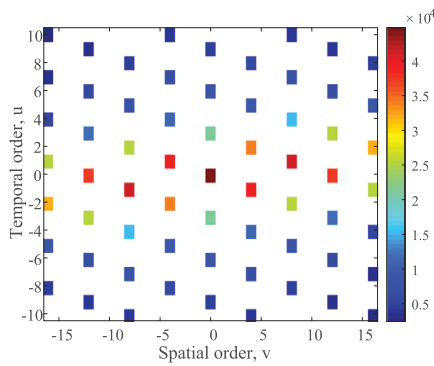**FIGURE 24.** Radial force density waveform for a 12/8 SRM.

FIGURE 25. FFT results of the radial force density waveform for a 12/8 SRM.

chopping mode. Additional improvements to the conventional two-stage commutation method can be found on [172]–[177].

Although the two-stage commutation method effectively reduces vibration, the introduced zero-voltage loop makes the demagnetization current period longer. Especially at high speed operation, the long tail current will likely generate negative torque and reduce efficiency. Additionally, this method only reduces the vibration at the dominant vibration mode.

B. CURRENT PROFILING

Because the radial force is a nonlinear function of phase current and rotor position, it can be controlled to a certain shape which could reduce vibration through the current profiling method, similarly to how this method is used for torque ripple reduction. In the existing literature, the current profiling method is mainly derived from two kinds of radial force shape.

The first kind of radial force shape is developed by eliminating the high temporal order of the radial force density FFT results [178]. A typical radial force density waveform for a three-phase 12/8 SRM is shown in Fig. 24 and its 2-dimensional FFT decomposition is given in Fig. 25. The radial force density was calculated by (9) based on the simulated B_r and B_t. The considered SRM is a three-phase 12/8 machine, with a rated torque of 3.69 Nm, a rated speed of 6000 rpm, and a bore radius of 41.8 mm.

According to the analysis in [28], the spatial order determines the shape of the excitation and the temporal order represents the forcing excitation frequency. The circumferential vibration modes of the stator only resonate with the same spatial orders of the radial force density wave. If the forcing frequency of the temporal order at a certain spatial order coincides with the natural frequency of the vibration modes corresponding to this certain spatial order, large vibration and loud acoustic noise will be generated. Thus, if the high order temporal order is eliminated, the noise at certain vibration modes will be reduced. It is found in [28] that the high order temporal order reduction in the radial force density waveform can be performed by shaping the phase radial force to a Gaussian shape. Based on this radial force shape constraint and other constraints, including torque ripple, a numerical optimization algorithm is used to obtain the phase reference current. Note that the Gaussian shape of radial force indicates the smooth and slow variation of the radial force.

On the other hand, the authors in [179] shape the sum of the radial force to reduce its third order harmonic for a three-phase SRM, suppressing the vibration at the resonance frequency. The current reference is assumed as (18):

$$i_{(\theta)} = I_0 + I_1 \sin(\theta_e) + I_2 \sin(2\theta_e) + I_3 \sin(3\theta_e) \qquad (18)$$

where I_0 and I_1 mainly affect the average torque and I_2 and I_3 are responsible for third order harmonic reduction. With the assumption that the SRM only operates at unsaturated conditions, the close form for this reference current can be analytically obtained.

By fitting the complete radial force characteristics with Fourier series, the method in [179] was extended to the saturated working conditions [180]. A simplified current reference of (18) which only contains the first three terms was presented in [181]. This simplified current reference shows lower torque ripple and lower RMS current when compared with the current reference in (18). Although the radical force is significantly reduced with the above-mentioned methods, other performance metrics, such as torque ripple and efficiency, should also be considered in the SRM drive system by optimizing the current reference. The phase shifts φ_2 and φ_3 were added to the second and third term in the current reference (18) [182] to develop the low torque ripple reference current and minimum RMS current reference. It is reported in [182] that the minimum RMS current reference shows better efficiency compared to the conventional squared current reference, but degrades the torque ripple performance. Moreover, the low torque ripple current reference in [182] shows good torque ripple reduction, however, it decreases the system efficiency slightly when compared with the conventional squared current reference. To achieve better system efficiency, the current reference was further improved by adding the phase φ_1 in [183]. Increased efficiency is found in the optimized current reference in [183] when compared to the square current reference. Achieving radial force suppression, torque ripple reduction and high system efficiency simultaneously is a complex task. To reach such a target, the reference current was modified to (19) in [184]. With proper numerical optimization, this
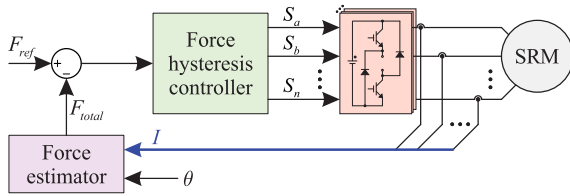
FIGURE 26. General block diagram for DIFC.

reference current can achieve low torque ripple, low sum of the radial force, and similar efficiency when compared with the conventional square reference current. More experimental verification of reference current (19) was recently reported in [185] and [186].

$$i_{(\theta)} = I_0 + I_1 \sin(\theta_e + \varphi_1) + I_2 \sin(2\theta_e + \varphi_2)$$
$$+ I_3 \sin(3\theta_e + \varphi_3) + I_4 \sin(4\theta_e + \varphi_4) \quad (19)$$

Other current profiling methods through numerical optimization to reduce the radial force ripple can be found in [185], [187]–[190]. To make the above current profiling methods clearer, they can be summarized as: (a) the methods presented in [121], [122], [181]–[186], [188]–[191] reduce the torque ripple and radial force simultaneously, and (b) the methods shown in [182]–[186] also considered the system efficiency.

C. DIRECT INSTANTANEOUS FORCE CONTROL

As in the case of the DITC method described earlier, the sum of the radial force can also be directly controlled. In [192], the authors pointed out that the mode 0 vibration is a prominent source of noise for larger sized SRM applications, such as electric vehicles, and this mode 0 vibration could be reduced by keeping the sum of the radial force as constant as possible. The outer average torque control loop provides the radial force reference and a feed-forward predicted radial force controller is used to regulate the radial force in [192]. A more commonly utilized DIFC implementation is described in Fig. 26, which not only avoids the inverse of radial force characteristics but also reduce the switching frequency [193], [194].

Although the mode-0 noise is indeed reduced with the above methods, the torque ripple is inevitably introduced since the radial force and torque characteristics differ a lot. To mitigate the radial force and torque ripple simultaneously, [195], [196] rearranged the radial force reference for the two conducting phases during the commutation period to reduce the torque ripple, at the cost of increased RMS current value when compared to the conventional method. Alternatively, [197]–[199] slightly modified the torque ripple minimization reference current by coordinating with the direct force controller, so the vibration is significantly reduced and the toque ripple is kept almost the same when compared with the results of torque ripple minimization controller.

D. COMPARISON OF THE VIBRATION SUPPRESSION METHODS

To effectively reduce the vibration and noise for a SRM, researchers have proposed different control methods from different perspectives. To better compare these methods, Table 3 summarizes these methods from the following aspects: advantages, disadvantages, need for radial force characteristics, and need for modal test.

The active vibration cancellation method works from the result of the varied phase radial force, which tries to suppress the vibration by introducing another vibration but with an inverse phase. Normally, this inverse vibration is generated by a proper period of the freewheeling mode after the turn-off instant. This method is easy to implement with the knowledge of the period for the dominant vibration mode. However, this method only works well for single pulse voltage control and is not able to reduce the torque ripple, which limits its application.

On the other hand, the current profiling method and DIFC method work on the generated radial force. The current profiling method shapes the phase radial force or the sum of the radial force to reduce vibration from different vibration modes. With different constraints, the generated reference current not only could reduce the vibration but also optimizes other objectives like torque ripple and efficiency. The drawbacks for this method lie on the time-cumbersome reference generation process, extra large memory space to store the reference current, and good current tracking requirement. The DIFC method straightforwardly controls the radial force as constant to reduce the mode-0 vibration, and the torque ripple can also be controlled at the same time. Compared with the current profiling method, it appears that the latter one shows better flexibility since DIFC only works on the mode-0 vibration on the present. Additionally, both of the current profiling method and the DIFC method require accurate radial force characteristics, but these characteristics cannot be measured directly and can only be obtained with complex indirect measurements [200]. Therefore, the study of obtaining the radial force characteristics is as important as the vibration suppression method itself.

VI. CONCLUSION AND FUTURE WORK

With the soaring development of transportation electrification, SRMs are gaining much interest in this field because of its rare-earth-free feature, simple and robust structure, and high reliability. Nevertheless, the high nonlinearity, pulsed torque feature, and unpleasant acoustic noise are barriers for the widespread use of SRMs.

For high-performance driving applications, good current tracking capability, smooth torque, and low noise emissions are essential. For decades, researchers have conducted intensive studies in the above-mentioned fields to enhance the performance of the SRM driving system. To clearly present these methods, this paper comprehensively reviews the existing advanced control methods regarding the current control, torque

TABLE 3. Summary and Comparison of the SRM Vibration Suppression Control Strategies

Method	Advantages	Disadvantages	Radial force characteristics	Modal test	Reference
Active vibration cancellation	Easy to implement, good noise reduction in single pulse voltage control	Only reduces the dominant vibration mode, less effective in low speed range, high torque ripple	No	Yes	[167]–[177]
Current profiling method	Effective in a wide speed range, able to reduce different vibration modes, torque ripple and efficiency can also be considered	Time-cumbersome to obtain the current reference, copper losses are possibly increased, requires accurate current tracking, might occupy significant memory to store the reference current	Yes	No	[121], [122], [178]–[185], [187]–[190]
DIFC	Effective in a wide speed range, torque ripple can also be considered	Only reduces the mode-0 vibration, copper losses is possibly increased	Yes	No	[192]–[199]

ripple reduction and vibration suppression. Additionally, the merits and drawbacks of each method are summarized and compared in detail.

In general, the current regulation strategies roughly consist of the model-independent methods and model-based methods. Since the incremental inductance and back-EMF are highly nonlinear terms, the model-independent methods have difficulty achieving good current regulation. On the contrary, with the accurate knowledge of the control plant, the model-based methods show excellent current control performance. As for the torque ripple reduction methods, indirect methods and direct methods are concurrent. The indirect methods seek for an appropriate current reference which not only reduces torque ripple but also might optimize other performance aspects, such as copper losses. On the other hand, the direct methods take advantage of the instantaneous torque feedback and generate proper switching signals to regulate the total torque. Regarding the vibration reduction, the active vibration cancellation method, current profiling method, and direct instantaneous force control method are reviewed. The active vibration cancellation method only reduces the dominant vibration mode under the single pulse voltage control but is simple to implement. The current profiling method is more flexible and could reduce several different vibration modes once the corresponding radial force reference form is known. Finally, the adoption of the DIFC method is beneficial on the mode 0 vibration reduction. Notably, most of the torque ripple reduction and vibration reduction method need accurate SRM model including torque characteristics and radial force characteristics.

Since the current controller is typically placed at the inner loop while the torque/radial force controller constitutes the outer loop, the above mentioned current controllers shows no interference with the torque/radial force controller. However, both the tangential force (torque) and radial force correlate to B_r and B_t. Hence, torque control interferes with the radial force control. Moreover, simultaneous control on the torque and radial force demands additional processing.

Based on the review results and the authors' knowledge, the following future research topics are essential for the widespread application of SRMs:

1) Minimal tracking error model-based current controller with low computational burden and tolerances to moderate model variation.
2) Robust torque control method with tolerances to model variation in a wide speed range.
3) Smooth radial force reference to reduce the vibration and torque ripple as much as possible without compromise on the average output torque and efficiency in a wide speed range.
4) Radial force characteristics estimation and robust instantaneous torque online estimation techniques.

REFERENCES

[1] J. O. Estima and A. J. Marques Cardoso, "Efficiency analysis of drive train topologies applied to electric/hybrid vehicles," *IEEE Trans. Veh. Technol.*, vol. 61, 3, no. 3, pp. 1021–1031, Mar. 2012.

[2] X. Liu, H. Chen, J. Zhao, and A. Belahcen, "Research on the performances and parameters of interior pmsm used for electric vehicles," *IEEE Trans. Ind. Electron.*, vol. 63, no. 6, pp. 3533–3545, Jun. 2016.

[3] E. Bostanci, M. Moallem, A. Parsapour, and B. Fahimi, "Opportunities and challenges of switched reluctance motor drives for electric propulsion: A comparative study," *IEEE Trans. Transport. Electrific.*, vol. 3, no. 1, pp. 58–75, Mar. 2017.

[4] Z. Xia *et al.*, "Computation-efficient online optimal tracking method for permanent magnet synchronous machine drives for mtpa and flux-weakening operations," *IEEE Trans. Emerg. Sel. Topics Power Electron.*, to be published, doi: 10.1109/JESTPE.2020.3039205.

[5] D. Xiao *et al.*, "Universal full-speed sensorless control scheme for interior permanent magnet synchronous motors," *IEEE Trans. Power Electron.*, vol. 36, no. 4, pp. 4723–4737, Apr. 2020.

[6] B. Bilgin, J. Jiang, and A. Emadi, *Switched Reluctance Motor Drives: Fundamentals to Applications*. Boca Raton, FL, USA: CRC Press, 2019.

[7] K. Kiyota and A. Chiba, "Design of switched reluctance motor competitive to 60-kw ipmsm in third-generation hybrid electric vehicle," *IEEE Trans. Ind. Appl.*, vol. 48, no. 6, pp. 2303–2309, Nov./Dec. 2012.

[8] I. Boldea, L. N. Tutelea, L. Parsa, and D. Dorrell, "Automotive electric propulsion systems with reduced or no permanent magnets: An overview," *IEEE Trans. Ind. Electron.*, vol. 61, no. 10, pp. 5696–5711, Oct. 2014.

[9] F. P. Scalcon *et al.*, "Robust control of synchronous reluctance motors by means of linear matrix inequalities," *IEEE Trans. Energy Convers.*, to be published, doi: 10.1109/TEC.2020.3028568

[10] C. Gan, J. Wu, Q. Sun, W. Kong, H. Li, and Y. Hu, "A review on machine topologies and control techniques for low-noise switched reluctance motors in electric vehicle applications," *IEEE Access*, vol. 6, pp. 31430–31443, 2018.

[11] B. Bilgin *et al.*, "Making the case for switched reluctance motors for propulsion applications," *IEEE Trans. Veh. Technol.*, vol. 69, no. 7, pp. 7172–7186, Jul. 2020.

[12] G. Fang, J. Ye, D. Xiao, Z. Xia, X. Wang, and A. Emadi, "Time-efficient torque shaping for switched reluctance machines from linear space," *IEEE Trans. Power Electron.*, to be published, doi: 10.1109/TPEL.2021.3056287.

[13] D. Xiao, J. Ye, G. Fang, Z. Xia, X. Wang, and A. Emadi, "Improved feature-position-based sensorless control scheme for srm drives based on nonlinear state observer at medium and high speeds," *IEEE Trans. Power Electron.*, vol. 36, no. 5, pp. 5711–5723, May 2021.

[14] Y. Sozer, I. Husain, and D. A. Torrey, "Guidance in selecting advanced control techniques for switched reluctance machine drives in emerging applications," *IEEE Trans. Ind. Appl.*, vol. 51, no. 6, pp. 4505–4514, Nov.-Dec. 2015.

[15] B. Singh, A. K. Mishra, and R. Kumar, "Solar powered water pumping system employing switched reluctance motor drive," *IEEE Trans. Ind. Appl.*, vol. 52, no. 5, pp. 3949–3957, Sept.-Oct. 2016.

[16] T. A. d. S. Barros, P. J. d. S. Neto, P. S. N. Filho, A. B. Moreira, and E. R. Filho, "An approach for switched reluctance generator in a wind generation system with a wide range of operation speed," *IEEE Trans. Power Electron.*, vol. 32, no. 11, pp. 8277–8292, Nov. 2017.

[17] F. Peng, J. Ye, A. Emadi, and Y. Huang, "Position sensorless control of switched reluctance motor drives based on numerical method," *IEEE Trans. Ind. Appl.*, vol. 53, no. 3, pp. 2159–2168, May/Jun. 2017.

[18] J. Borg Bartolo, M. Degano, J. Espina, and C. Gerada, "Design and initial testing of a high-speed 45-kw switched reluctance drive for aerospace application," *IEEE Trans. Ind. Electron.*, vol. 64, no. 2, pp. 988–997, Feb. 2017.

[19] C. R. D. Osório, F. P. Scalcon, R. P. Vieira, V. F. Montagner, and H. A. Gründling, "Robust control of switched reluctance generator in connection with a grid-tied inverter," in *Proc. IEEE 15th Braz. Power Electron. Conf. 5th IEEE Southern Power Electron. Conf.*, 2019, pp. 1–6.

[20] B. Bilgin, A. Emadi, and M. Krishnamurthy, "Comprehensive evaluation of the dynamic performance of a 6/10 srm for traction application in phevs," *IEEE Trans. Ind. Electron.*, vol. 60, no. 7, pp. 2564–2575, Jul. 2013.

[21] Z. Yang, F. Shang, I. P. Brown, and M. Krishnamurthy, "Comparative study of interior permanent magnet, induction, and switched reluctance motor drives for ev and hev applications," *IEEE Trans. Transport. Electrific.*, vol. 1, no. 3, pp. 245–254, Oct. 2015.

[22] E. Öksüztepe, "In-wheel switched reluctance motor design for electric vehicles by using a pareto-based multiobjective differential evolution algorithm," *IEEE Trans. Veh. Technol.*, vol. 66, no. 6, pp. 4706–4715, Jun. 2017.

[23] J. Zhu, K. W. E. Cheng, X. Xue, and Y. Zou, "Design of a new enhanced torque in-wheel switched reluctance motor with divided teeth for electric vehicles," *IEEE Trans. Magn.*, vol. 53, no. 11, pp. 1–4, Nov. 2017, Art. no. 2501504.

[24] B. Howey, B. Bilgin, and A. Emadi, "Design of an external-rotor direct drive e-bike switched reluctance motor," *IEEE Trans. Veh. Technol.*, vol. 69, no. 3, pp. 2552–2562, 2020.

[25] L. Ge, B. Burkhart, and R. W. De Doncker, "Fast iron loss and thermal prediction method for power density and efficiency improvement in switched reluctance machines," *IEEE Trans. Ind. Electron.*, vol. 67, no. 6, pp. 4463–4473, Mar. 2019.

[26] L. Ge, I. Ralev, A. Klein-Hessling, S. Song, and R. W. De Doncker, "A simple reluctance calibration strategy to obtain the flux-linkage characteristics of switched reluctance machines," *IEEE Trans. Power Electron.*, vol. 35, no. 3, pp. 2787–2798, Mar. 2019.

[27] I. Husain, "Minimization of torque ripple in srm drives," *IEEE Trans. Ind. Electron.*, vol. 49, no. 1, pp. 28–39, Feb. 2002.

[28] A. Dorneles Callegaro, J. Liang, J. W. Jiang, B. Bilgin, and A. Emadi, "Radial force density analysis of switched reluctance machines: The source of acoustic noise," *IEEE Trans. Transport. Electrific.*, vol. 5, no. 1, pp. 93–106, Mar. 2019.

[29] B. Bilgin and A. Emadi, "Electric motors in electrified transportation: A step toward achieving a sustainable and highly efficient transportation system," *IEEE Power Electron. Mag.*, vol. 1, no. 2, pp. 10–17, Jun. 2014.

[30] D. F. Valencia, R. Tarvirdilu-Asl, C. Garcia, J. Rodriguez, and A. Emadi, "A review of predictive control techniques for switched reluctance machine drives. part i: Fundamentals and current control," *IEEE Trans. Energy Convers.*, to be published, doi: 10.1109/TEC.2020.3047983.

[31] S. Song, G. Fang, Z. Zhang, R. Ma, and W. Liu, "Unsaturated-inductance-based instantaneous torque online estimation of switched reluctance machine with locally linearized energy conversion loop," *IEEE Trans. Ind. Electron.*, vol. 65, no. 8, pp. 6109–6119, Aug. 2018.

[32] F. R. Salmasi and B. Fahimi, "Modeling switched-reluctance machines by decomposition of double magnetic saliencies," *IEEE Trans. Magn.*, vol. 40, no. 3, pp. 1556–1561, May 2004.

[33] H. Gao, F. R. Salmasi, and M. Ehsani, "Inductance model-based sensorless control of the switched reluctance motor drive at low speed," *IEEE Trans. Power Electron.*, vol. 19, no. 6, pp. 1568–1573, Nov. 2004.

[34] J. Ye, B. Bilgin, and A. Emadi, "Elimination of mutual flux effect on rotor position estimation of switched reluctance motor drives considering magnetic saturation," *IEEE Trans. Power Electron.*, vol. 30, no. 2, pp. 532–536, Feb. 2015.

[35] F. Peng, J. Ye, and A. Emadi, "An asymmetric three-level neutral point diode clamped converter for switched reluctance motor drives," *IEEE Trans. Power Electron.*, vol. 32, no. 11, pp. 8618–8631, Nov. 2017.

[36] F. Peng and A. Emadi, "A digital pwm current controller for switched reluctance motor drives," in *Proc. IEEE Transp. Electrific. Conf. Expo.*, 2014, pp. 1–6.

[37] N. C. Sahoo, J. X. Xu, and S. K. Panda, "Low torque ripple control of switched reluctance motors using iterative learning," *IEEE Trans. Energy Convers.*, vol. 16, no. 4, pp. 318–326, Dec. 2001.

[38] S. K. Sahoo, S. K. Panda, and J. X. Xu, "Iterative learning-based high-performance current controller for switched reluctance motors," *IEEE Trans. Energy Convers.*, vol. 19, no. 3, pp. 491–498, Sep. 2004.

[39] Y. Zheng, H. Sun, Y. Dong, and P. Li, "A current control method of switched reluctance motors based on iterative learning control considering the mutual inductance," in *Proc. Int. Conf. Elect. Mach. Syst.*, 2008, pp. 3401–3404.

[40] Z. Yi, X. Li, S. Hexu, and D. Yan, "An optimal torque controller based on iterative learning control for switched reluctance motors for electric vehicles," in *Proc. Int. Conf. Optoelectron. Image Process.*, vol. 1, 2010, pp. 230–233.

[41] C. Lai, Y. Zheng, A. Labak, and N. C. Kar, "Investigation and analysis of iterative learning-based current control algorithm for switched reluctance motor applications," in *Proc. Int. Conf. Elect. Mach.*, 2014, pp. 796–802.

[42] H. Alharkan, P. Shamsi, S. Saadatmand, and M. Ferdowsi, "Q-learning scheduling for tracking current control of switched reluctance motor drives," in *Proc. IEEE Power Energy Conf.*, 2020, pp. 1–6.

[43] I. Husain and M. Ehsani, "Torque ripple minimization in switched reluctance motor drives by pwm current control," *IEEE Trans. Power Electron.*, vol. 11, no. 1, pp. 83–88, Jan. 1996.

[44] G. Baoming and Z. Nan, "Dsp-based discrete-time reaching law control of switched reluctance motor," in *Proc. CES/IEEE 5th Int. Power Electron. Motion Control Conf.*, vol. 2, 2006, pp. 1–5.

[45] M. Ilic'-Spong, R. Marino, S. Peresada, and D. Taylor, "Feedback linearizing control of switched reluctance motors," *IEEE Trans. Autom. Control*, vol. 32, no. 5, pp. 371–379, May 1987.

[46] M. W. Arab, E. Godoy, I. Bahri, M. Hilairet, P. G. Estébanez, and S. A. Randi, "Current controller for switched reluctance motors using pole placement approach," in *Proc. Int. Electric Mach. Drives Conf.*, 2013, pp. 1119–1125.

[47] X. Wang and J.-S. Lai, "Small-signal modeling and control for pwm control of switched reluctance motor drives," in *Proc. IEEE 33rd Annu. IEEE Power Electron. Specialists Conf.*, vol. 22002, pp. 546–551.

[48] R. Banerjee, M. Sengupta, and S. Dalapati, "Design and implementation of current mode control in a switched reluctance drive," in *Proc. IEEE Int. Conf. Power Electron., Drives Energy Syst.*, 2014, pp. 1–5.

[49] R. M. Milasi and M. Moallem, "A novel multi-loop self-tunning adaptive pi control scheme for switched reluctance motors," in *Proc. IECON 40th Annu. Conf. IEEE Ind. Electron. Soc.*, 2014, pp. 337–342.

[50] S. S. Ahmad and G. Narayanan, "Linearized modeling of switched reluctance motor for closed-loop current control," *IEEE Trans. Ind. Appl.*, vol. 52, no. 4, pp. 3146–3158, Aug. 2016.

[51] S. E. Schulz and K. M. Rahman, "High-performance digital pi current regulator for ev switched reluctance motor drives," *IEEE Trans. Ind. Appl.*, vol. 39, no. 4, pp. 1118–1126, Jul./Aug. 2003.

[52] G. Schroder and J. Bekiesch, "Adaptive current control for the srm," in *Proc. IEEE Int. Symp. Ind. Electron.*, vol. 1, 2005, pp. 69–74.

[53] Z. Lin, D. Reay, B. Williams, and X. He, "High-performance current control for switched reluctance motors based on on-line estimated parameters," *IET Electric Power Appl.*, vol. 4, no. 1, pp. 67–74, 2010.

[54] H. Huang, K. Hu, Y. Wu, T. Jong, and C. Liaw, "A current control scheme with back emf cancellation and tracking error adapted commutation shift for switched-reluctance motor drive," *IEEE Trans. Ind. Electron.*, vol. 63, no. 12, pp. 7381–7392, Dec. 2016.

[55] H. Hannoun, M. Hilairet, and C. Marchand, "Gain-scheduling pi current controller for a switched reluctance motor," in *Proc. IEEE Int. Symp. Ind. Electron.*, 2007, pp. 1177–1182.

[56] N. Ouddah, M. Boukhnifer, A. Chaibet, and E. Monmasson, "Robust lpv current control of switched reluctance motors," in *Proc. 22nd Mediterranean Conf. Control Automat.*, 2014, pp. 218–223.

[57] J. Song, S. Song, and B. Qu, "Application of an adaptive pi controller for a switched reluctance motor drive," in *Proc. IEEE 2nd Annu. Southern Power Electron. Conf.*, 2016, pp. 1–5.

[58] R. Mikail, I. Husain, Y. Sozer, M. Islam, and T. Sebastian, "A fixed switching frequency predictive current control method for switched reluctance machines," in *Proc. IEEE Energy Convers. Congr. Expo.*, 2012, pp. 843–847.

[59] R. Mikail, I. Husain, Y. Sozer, M. S. Islam, and T. Sebastian, "A fixed switching frequency predictive current control method for switched reluctance machines," *IEEE Trans. Ind. Appl.*, vol. 50, no. 6, pp. 3717–3726, Nov.-Dec. 2014.

[60] M. Ma, Q. Yang, X. Zhang, F. Li, and Z. Lin, "A switched reluctance motor torque ripple reduction strategy with deadbeat current control," in *Proc. 14th IEEE Conf. Ind. Electron. Appl.*, 2019, pp. 25–30.

[61] S. Mehta, I. Husain, and P. Pramod, "Predictive current control of mutually coupled switched reluctance motors using net flux method," in *Proc. IEEE Energy Convers. Congr. Expo.*, 2019, pp. 4918–4922.

[62] X. Zhang, Q. Yang, M. Ma, Z. Lin, and S. Yang, "A switched reluctance motor torque ripple reduction strategy with deadbeat current control and active thermal management," *IEEE Trans. Veh. Technol.*, vol. 69, no. 1, pp. 317–327, Jan. 2020.

[63] S. S. Ahmad and G. Narayanan, "Predictive control based constant current injection scheme for characterization of switched reluctance machine," *IEEE Trans. Ind. Appl.*, vol. 54, no. 4, pp. 3383–3392, Jul./Aug. 2018.

[64] J. Taylor, D. F. Valencia, B. Bilgin, M. Narimani, and A. Emadi, "Comparison of current control strategies for low- and high-power switched reluctance motor drives," in *Proc. IEEE Transp. Electrific. Conf. Expo.*, 2020, pp. 198–203.

[65] J. Rodriguez *et al.*, "State of the art of finite control set model predictive control in power electronics," *IEEE Trans. Ind. Informat.*, vol. 9, no. 2, pp. 1003–1016, May 2013.

[66] C. R. D. Osório, G. S. da Silva, J. C. Giacomini, and C. Rech, "Comparative analysis of predictive current control techniques applied to single-phase grid-connected inverters," in *Proc. Braz. Power Electron. Conf.*, 2017, pp. 1–6.

[67] M. Kiani, "Model predictive control of stator currents in switched reluctance generators," in *Proc. IEEE 23rd Int. Symp. Ind. Electron.*, 2014, pp. 842–846.

[68] X. Li and P. Shamsi, "Inductance surface learning for model predictive current control of switched reluctance motors," *IEEE Trans. Transport. Electrific.*, vol. 1, no. 3, pp. 287–297, Oct. 2015.

[69] X. Li and P. Shamsi, "Model predictive current control of switched reluctance motors with inductance auto-calibration," *IEEE Trans. Ind. Electron.*, vol. 63, no. 6, pp. 3934–3941, Jun. 2016.

[70] S. Mehta, M. A. Kabir, and I. Husain, "Extended speed current profiling algorithm for low torque ripple srm using model predictive control," in *Proc. IEEE Energy Convers. Congr. Expo.*, 2018, pp. 4558–4563.

[71] D. F. Valencia, S. R. Filho, A. D. Callegaro, M. Preindl, and A. Emadi, "Virtual-flux finite control set model predictive control of switched reluctance motor drives," in *Proc. IECON 45th Annu. Conf. IEEE Ind. Electron. Soc.*, vol. 1, 2019, pp. 1465–1470.

[72] X. Li and P. Shamsi, "Adaptive model predictive current control for dssrm drives," in *Proc. IEEE Transp. Electrific. Conf. Expo.*, 2014, pp. 1–5.

[73] K. Hu, L. Guo, and J. Ye, "Model predictive current control of mutually coupled switched reluctance machines using a three-phase voltage source converter," in *Proc. IEEE Appl. Power Electron. Conf. Expo.*, 2020, pp. 704–710.

[74] H. Naitoh and H. Ishikawa, "A current controller for a switched reluctance motor based on model reference adaptive control," in *SPEEDAM*, 2010, pp. 1270–1275.

[75] F. Peng, J. Ye, and A. Emadi, "A digital pwm current controller for switched reluctance motor drives," *IEEE Trans. Power Electron.*, vol. 31, no. 10, pp. 7087–7098, Oct. 2016.

[76] I. S. Manolas, A. X. Kaletsanos, and S. N. Manias, "Nonlinear current control technique for high performance switched reluctance machine drives," in *Proc. IEEE Power Electron. Specialists Conf.*, 2008, pp. 1229–1234.

[77] I. Manolas, G. Papafotiou, and S. N. Manias, "Sliding mode pwm for effective current control in switched reluctance machine drives," in *Proc. Int. Power Electron. Conf.*, 2014, pp. 1606–1612.

[78] Z. Ruiwei, Q. Xisen, J. Liping, Z. Yingchao, Z. Tianwen, and N. Jintong, "An adaptive sliding mode current control for switched reluctance motor," in *Proc. IEEE Conf. Expo. Transp. Electrific.*, 2014, pp. 1–6.

[79] X. Yao, R. Qi, Z. Deng, and J. Cai, "High-performance torque control for switched reluctance motor based on online fuzzy neural network modeling," in *Proc. Int. Conf. Intell. Syst. Des. Eng. Appl.*, vol. 1, 2010, pp. 817–822.

[80] Y. Yang and Y. Zhang, "Sliding mode-pi control of switched reluctance motor drives for ev," in *Proc. Int. Conf. Elect. Mach. Syst.*, vol. 1, 2005, pp. 603–607.

[81] J. Ye, P. Malysz, and A. Emadi, "A fixed-switching-frequency integral sliding mode current controller for switched reluctance motor drives," *IEEE Trans. Emerg. Sel. Topics Power Electron.*, vol. 3, no. 2, pp. 381–394, Jun. 2015.

[82] K. Hu, J. Ye, J. M. Velni, L. Guo, and B. Yang, "A fixed-switching-frequency sliding mode current controller for mutually coupled switched reluctance machines using asymmetric bridge converter," in *Proc. IEEE Transp. Electrific. Conf. Expo.*, 2019, pp. 1–6.

[83] K. Hu, J. Ye, and J. M. Velni, "Sliding mode current control of mutually coupled switched reluctance machines using a three-phase voltage source converter," in *Proc. IEEE Energy Convers. Congr. Expo.*, 2019, pp. 1776–1781.

[84] X. Rain, M. Hilairet, and R. Talj, "Second order sliding mode current controller for the switched reluctance machine," in *Proc. IECON 36th Annu. Conf. IEEE Ind. Electron. Soc.*, 2010, pp. 3301–3306.

[85] F. B. Salem, I. Bahri, H. Maamri, and N. Derbel, "A second-order sliding mode control of switched reluctance motor," *Electric Power Compon. Syst.*, vol. 48, no. 6-7, pp. 640–651, 2020.

[86] M. Ilić-Spong, T. J. E. Miller, S. R. MacMinn, and J. S. Thorp, "Instantaneous torque control of electric motor drives," in *Proc. IEEE Power Electron. Specialists Conf.*, 1985, pp. 42–48.

[87] D. S. Schramm, B. W. Williams, and T. C. Green, "Torque ripple reduction of switched reluctance motors by phase current optimal profiling," in *Proc. PESC Record. 23rd Annu. IEEE Power Electron. Specialists Conf.* vol. 2, 1992, pp. 857–860.

[88] N. C. Sahoo, J. X. Xu, and S. K. Panda, "Determination of current waveforms for torque ripple minimisation in switched reluctance motors using iterative learning: An investigation," *IEE Proc. - Electric Power Appl.*, vol. 146, no. 4, pp. 369–377, 1999.

[89] X. D. Xue, K. W. E. Cheng, and S. L. Ho, "Optimization and evaluation of torque-sharing functions for torque ripple minimization in switched reluctance motor drives," *IEEE Trans. Power Electron.*, vol. 24, no. 9, pp. 2076–2090, Sep. 2009.

[90] V. P. Vujičić, "Minimization of torque ripple and copper losses in switched reluctance drive," *IEEE Trans. Power Electron.*, vol. 27, no. 1, pp. 388–399, Jan. 22012.

[91] A. K. Rana and A. Raviteja, "A mathematical torque ripple minimization technique based on nonlinear modulating factor for switched reluctance motor drives," *IEEE Trans. Ind. Electron.*, to be published, doi: 10.1109/TIE.2021.3063871.

[92] K. J. Tseng and S. Cao, "A srm variable speed drive with torque ripple minimization control," in *Proc. APEC 16th Annu. IEEE Appl. Power Electron. Conf. Expo.*, vol. 2, 2001, pp. 1083–1089.

[93] Q. Sun, J. Wu, C. Gan, Y. Hu, and J. Si, "Octsf for torque ripple minimisation in srms," *IET Power Electron.*, vol. 9, no. 14, pp. 2741–2750, 2016.

[94] D. Lee, S.-Y. Ahn, J.Ahn, and Jang-MokKim, "Modified tsf for the high speed switched reluctance motor," in *Proc. IEEE Int. Symp. Ind. Electron.*, 2011, pp. 655–660.

[95] M. Dowlatshahi, S. M. S. Nejad, and J. Ahn, "Torque ripple minimization of switched reluctance motor using modified torque sharing function," in *Proc. 21st Iranian Conf. Elect. Eng.*, 2013, pp. 1–6.

[96] C. Gan, Q. Sun, Y. Chen, J. Si, J. Wu, and Y. Hu, "A position sensorless torque control strategy for switched reluctance machines with fewer current sensors," *IEEE/ASME Trans. Mechatronics*, vol. 26, no. 2, pp. 1118–1128, Apr. 2021.

[97] H.-S. Ro, K.-G. Lee, J.-S. Lee, H.-G. Jeong, and K.-B. Lee, "Torque ripple minimization scheme using torque sharing function based fuzzy logic control for a switched reluctance motor," *J. Elect. Eng. Technol.*, vol. 10, no. 1, pp. 118–127, 2015.

[98] D. Lee, J. Liang, Z. Lee, and J. Ahn, "A simple nonlinear logical torque sharing function for low-torque ripple sr drive," *IEEE Trans. Ind. Electron.*, vol. 56, no. 8, pp. 3021–3028, Aug. 2009.

[99] J. Ye, B. Bilgin, and A. Emadi, "An extended-speed low-ripple torque control of switched reluctance motor drives," *IEEE Trans. Power Electron.*, vol. 30, no. 3, pp. 1457–1470, Mar. 2015.

[100] S. K. Sahoo, S. K. Panda, and Jian-Xin Xu, "Indirect torque control of switched reluctance motors using iterative learning control," *IEEE Trans. Power Electron.*, vol. 20, no. 1, pp. 200–208, Jan. 2005.

[101] Z. Lin, D. S. Reay, B. W. Williams, and X. He, "Torque ripple reduction in switched reluctance motor drives using b-spline neural networks," *IEEE Trans. Ind. Appl.*, vol. 42, no. 6, pp. 1445–1453, Nov.-Dec. 2006.

[102] H. Lovatt and J. Stephenson, "Computer-optimised smooth-torque current waveforms for switched-reluctance motors," *IEE Electric Power Appl.*, vol. 144, no. 5, pp. 310–316, 1997.

[103] C. Choi, S. Kim, Y. Kim, and K. Park, "A new torque control method of a switched reluctance motor using a torque-sharing function," *IEEE Trans. Magn.*, vol. 38, no. 5, pp. 3288–3290, Sep. 2002.

[104] J. Ye, B. Bilgin, and A. Emadi, "An offline torque sharing function for torque ripple reduction in switched reluctance motor drives," *IEEE Trans. Energy Convers.*, vol. 30, no. 2, pp. 726–735, Jun. 2015.

[105] H. Li, B. Bilgin, and A. Emadi, "An improved torque sharing function for torque ripple reduction in switched reluctance machines," *IEEE Trans. Power Electron.*, vol. 34, no. 2, pp. 1635–1644, Feb. 2019.

[106] Z. Xia, B. Bilgin, S. Nalakath, and A. Emadi, "A new torque sharing function method for switched reluctance machines with lower current tracking error," *IEEE Trans. Ind. Electron.*, to be published, doi: 10.1109/TIE.2020.3037987.

[107] R. S. Wallace and D. G. Taylor, "A balanced commutator for switched reluctance motors to reduce torque ripple," *IEEE Trans. Power Electron.*, vol. 7, no. 4, pp. 617–626, Oct. 1992.

[108] R. Mikail, I. Husain, Y. Sozer, M. S. Islam, and T. Sebastian, "Torque-ripple minimization of switched reluctance machines through current profiling," *IEEE Trans. Ind. Appl.*, vol. 49, no. 3, pp. 1258–1267, May/Jun. 2013.

[109] R. Mikail, I. Husain, M. S. Islam, Y. Sozer, and T. Sebastian, "Four-quadrant torque ripple minimization of switched reluctance machine through current profiling with mitigation of rotor eccentricity problem and sensor errors," *IEEE Trans. Ind. Appl.*, vol. 51, no. 3, pp. 2097–2104, May/Jun. 2015.

[110] T. Kusumi, T. Hara, K. Umetani, and E. Hiraki, "Simultaneous tuning of rotor shape and phase current of switched reluctance motors for eliminating input current and torque ripples with reduced copper loss," *IEEE Trans. Ind. Appl.*, vol. 56, no. 6, pp. 6384–6398, Nov./Dec. 2020.

[111] P. L. Chapman and S. D. Sudhoff, "Design and precise realization of optimized current waveforms for an 8/6 switched reluctance drive," *IEEE Trans. Power Electron.*, vol. 17, no. 1, pp. 76–83, Jan. 2002.

[112] J. Chai and C. Liaw, "Reduction of speed ripple and vibration for switched reluctance motor drive via intelligent current profiling," *IET Electric Power Appl.*, vol. 4, no. 5, pp. 380–396, 2010.

[113] S. Mir, M. E. Elbuluk, and I. Husain, "Torque-ripple minimization in switched reluctance motors using adaptive fuzzy control," *IEEE Trans. Ind. Appl.*, vol. 35, no. 2, pp. 461–468, Mar./Apr. 1999.

[114] C. Shang, D. Reay, and B. Williams, "Adapting cmac neural networks with constrained lms algorithm for efficient torque ripple reduction in switched reluctance motors," *IEEE Trans. Control Syst. Technol.*, vol. 7, no. 4, pp. 401–413, Jul. 1999.

[115] L. O. d. A. P. Henriques, P. C. Branco, L. G. B. Rolim, and W. I. Suemitsu, "Proposition of an offline learning current modulation for torque-ripple reduction in switched reluctance motors: Design and experimental evaluation," *IEEE Trans. Ind. Electron.*, vol. 49, no. 3, pp. 665–676, Jun. 2002.

[116] Z. Q. Zhu, B. Lee, L. Huang, and W. Chu, "Contribution of current harmonics to average torque and torque ripple in switched reluctance machines," *IEEE Trans. Magn.*, vol. 53, no. 3, pp. 1–9, Mar. 2017, Art. no. 8100909.

[117] X. Liu, Z. Zhu, and Z. Pan, "Analysis of electromagnetic torque in sinusoidal excited switched reluctance machines having dc bias in excitation," in *Proc. 20th Int. Conf. Elect. Machines*, 2012, pp. 2882–2888.

[118] J. Stephenson, A. Hughes, and R. Mann, "Torque ripple minimisation in a switched reluctance motor by optimum harmonic current injection," *IEE Proc.-Electric Power Appl.*, vol. 148, no. 4, pp. 322–328, 2001.

[119] J. Stephenson, A. Hughes, and R. Mann, "Online torque-ripple minimisation in a switched reluctance motor over a wide speed range," *IEE Proc.-Electric Power Appl.*, vol. 149, no. 4, pp. 261–267, 2002.

[120] N. T. Shaked and R. Rabinovici, "New procedures for minimizing the torque ripple in switched reluctance motors by optimizing the phase-current profile," *IEEE Trans. Magn.*, vol. 41, no. 3, pp. 1184–1192, Mar. 2005.

[121] C. Ma, L. Qu, R. Mitra, P. Pramod, and R. Islam, "Vibration and torque ripple reduction of switched reluctance motors through current profile optimization," in *Proc. IEEE Appl. Power Electron. Conf. Expo.*, 2016, pp. 3279–3285.

[122] O. Gundogmus, Y. Sozer, L. Vadamodala, J. Kutz, J. Tylenda, and R. L. Wright, "Current harmonics injection method for simultaneous torque and radial force ripple mitigation to reduce acoustic noise and vibration in srms," in *Proc. IEEE Energy Convers. Congr. Expo.*, 2019, pp. 7091–7097.

[123] M. Ma, F. Ling, F. Li, and F. Liu, "Torque ripple suppression of switched reluctance motor by segmented harmonic currents injection based on adaptive fuzzy logic control," *IET Electric Power Appl.*, vol. 14, no. 2, pp. 325–335, 2019.

[124] X. Z. Liu, G. C. Verghese, J. H. Lang, and M. Onder, "Generalizing the blondel-park transformation of electrical machines: Necessary and sufficient conditions," *IEEE Trans. Circuits Syst.*, vol. 36, no. 8, pp. 1058–1067, Aug. 1989.

[125] N. J. Nagel and R. D. Lorenz, "Rotating vector methods for smooth torque control of a switched reluctance motor drive," *IEEE Trans. Ind. Appl.*, vol. 36, no. 2, pp. 540–548, Mar./Apr. 2000.

[126] N. J. Nagel and R. D. Lorenz, "Complex rotating vector method for smooth torque control of a saturated switched reluctance motor," in *Proc. 34th Conf. Record IEEE Ind. Appl. Conf. IAS Ann. Meeting*, vol. 4, 1999, pp. 2591–2598.

[127] T. Husain, A. Elrayyah, Y. Sozer, and I. Husain, "Flux-weakening control of switched reluctance machines in rotating reference frame," *IEEE Trans. Ind. Appl.*, vol. 52, no. 1, pp. 267–277, Jan.-Feb. 2016.

[128] W. Ding, G. Liu, and P. Li, "A hybrid control strategy of hybrid-excitation switched reluctance motor for torque ripple reduction and constant power extension," *IEEE Trans. Ind. Electron.*, vol. 67, no. 1, pp. 38–48, Jan. 2020.

[129] X. Liu *et al.*, "Performance comparison between unipolar and bipolar excitations in switched reluctance machine with sinusoidal and rectangular waveforms," in *Proc. IEEE Energy Convers. Congr. Expo.*, 2011, pp. 1590–1595.

[130] N. Nakao and K. Akatsu, "Vector control specialized for switched reluctance motor drives," in *Proc. Int. Conf. Elect. Machines*, 2014, pp. 943–949.

[131] N. Nakao and K. Akatsu, "Vector control for switched reluctance motor drives using an improved current controller," in *Proc. IEEE Energy Convers. Congr. Expo.*, 2014, pp. 1379–1386.

[132] S. Kuai, H. Zhang, X. Xia, and K. Li, "Unipolar sinusoidal excited switched reluctance motor control based on voltage space vector," *IET Electric Power Appl.*, vol. 13, no. 5, pp. 670–675, 2018.

[133] S. Kuai, X. Xia, H. Zhang, and K. Hu, "Low-torque ripple control of srm based on current vector," *IET Electric Power Appl.*, vol. 14, no. 4, pp. 723–730, 2020.

[134] Z. Yu, C. Gan, Y. Chen, and R. Qu, "Dc-biased sinusoidal current excited switched reluctance motor drives based on flux modulation principle," *IEEE Trans. Power Electron.*, vol. 35, no. 10, pp. 10614–10628, Oct. 2020.

[135] R. Inderka and R. De Doncker, "Ditc-direct instantaneous torque control of switched reluctance drives," in *Proc. Conf. Record 37th IEEE Ind. Appl. Conf. IAS Annu. Meeting*, vol. 3, 2002, pp. 1605–1609.

[136] R. B. Inderka and R. W. De Doncker, "Ditc-direct instantaneous torque control of switched reluctance drives," *IEEE Trans. Ind. Appl.*, vol. 39, no. 4, pp. 1046–1051, Jul./Aug. 2003.

[137] N. H. Fuengwarodsakul, M. Menne, R. B. Inderka, and R. W. De Doncker, "High-dynamic four-quadrant switched reluctance drive based on DITC," *IEEE Trans. Ind. Appl.*, vol. 41, no. 5, pp. 1232–1242, Sept./Oct. 2005.

[138] C. R. Neuhaus, N. H. Fuengwarodsakul, and R. W. De Doncker, "Predictive pwm-based direct instantaneous torque control of switched reluctance drives," in *Proc. 37th IEEE Power Electron. Specialists Conf.*, 2006, pp. 1–7.

[139] M. V. d. Paula and T. A. Dos Santos Barros, "A sliding mode ditc cruise control for srm with steepest descent minimum torque ripple point tracking," *IEEE Trans. Ind. Electron.*, to be published, doi: 10.1109/TIE.2021.3050349.

[140] M. V. de Paula, T. A. d. S. Barros, H. S. Moreira, E. H. Catata, M. G. Villalva, and E. R. Filho, "A dahlin cruise control design method for switched reluctance motors with minimum torque ripple point tracking applied in electric vehicles," *IEEE Trans. Transport. Electrific.*, to be published, doi: 10.1109/TTE.2020.3019997.

[141] Y. Wang, H. Wu, W. Zhang, and Y. Ma, "A high efficiency direct instantaneous torque control of srm using commutation angles control," in *Proc. 17th Int. Conf. Elect. Machines Syst.*, 2014, pp. 2863–2866.

[142] Q. Sun, J. Wu, and C. Gan, "Optimized direct instantaneous torque control for srms with efficiency improvement," *IEEE Trans. Ind. Electron.*, vol. 68, no. 3, pp. 2072–2082, Mar. 2021.

[143] S. Yao and W. Zhang, "A simple strategy for parameters identification of srm direct instantaneous torque control," *IEEE Trans. Power Electron.*, vol. 33, no. 4, pp. 3622–3630, Apr. 2018.

[144] S. Song, G. Fang, R. Hei, J. Jiang, R. Ma, and W. Liu, "Torque ripple and efficiency online optimization of switched reluctance machine based on torque per ampere characteristics," *IEEE Trans. Power Electron.*, vol. 35, no. 9, pp. 9610–9618, Sept. 2020.

[145] H. J. Brauer, M. D. Hennen, and R. W. De Doncker, "Control for polyphase switched reluctance machines to minimize torque ripple and decrease ohmic machine losses," *IEEE Trans. Power Electron.*, vol. 27, no. 1, pp. 370–378, Jan. 2012.

[146] J. Liang, D.-H. Lee, and J.-W. Ahn, "Direct instantaneous torque control of switched reluctance machines using 4-level converters," *IET Electric Power Appl.*, vol. 3, no. 4, pp. 313–323, 2009.

[147] S. Song, C. Peng, Z. Guo, R. Ma, and W. Liu, "Direct instantaneous torque control of switched reluctance machine based on modular multi-level power converter," in *Proc. 22nd Int. Conf. Elect. Machines Syst.*, 2019, pp. 1–6.

[148] H. Zeng, H. Chen, and J. Shi, "Direct instantaneous torque control with wide operating range for switched reluctance motors," *IET Electric Power Appl.*, vol. 9, no. 9, pp. 578–585, 2015.

[149] T. Husain, A. Elrayyah, Y. Sozer, and I. Husain, "Unified control for switched reluctance motors for wide speed operation," *IEEE Trans. Ind. Electron.*, vol. 66, no. 5, pp. 3401–3411, May 2019.

[150] C. Gan, J. Wu, Q. Sun, S. Yang, Y. Hu, and L. Jin, "Low-cost direct instantaneous torque control for switched reluctance motors with bus current detection under soft-chopping mode," *IET Power Electron.*, vol. 9, no. 3, pp. 482–490, 2016.

[151] A. D. Cheok and Y. Fukuda, "A new torque and flux control method for switched reluctance motor drives," *IEEE Trans. Power Electron.*, vol. 17, no. 4, pp. 543–557, Jul. 2002.

[152] H.-J. Guo, "Considerations of direct torque control for switched reluctance motors," in *Proc. IEEE Int. Symp. Ind. Electron.*, vol. 3, 2006, pp. 2321–2325.

[153] X. Ai-De, Z. Xianchao, H. Kunlun, and C. Yuzhao, "Torque-ripple reduction of srm using optimised voltage vector in DTC," *IET Elect. Syst. Transp.*, vol. 8, no. 1, pp. 35–43, 2018.

[154] X. Deng, B. Mecrow, H. Wu, and R. Martin, "Design and development of low torque ripple variable-speed drive system with six-phase switched reluctance motors," *IEEE Trans. Energy Convers.*, vol. 33, no. 1, pp. 420–429, Mar. 2018.

[155] A. Xu, C. Shang, J. Chen, J. Zhu, and L. Han, "A new control method based on DTC and MPC to reduce torque ripple in SRM," *IEEE Access*, vol. 7, pp. 68 584–68 593, 2019.

[156] P. K. Reddy, D. Ronanki, and P. Perumal, "Efficiency improvement and torque ripple minimisation of four-phase switched reluctance motor drive using new direct torque control strategy," *IET Electric Power Appl.*, vol. 14, no. 1, pp. 52–61, 2019.

[157] X. Zhao, A. Xu, and W. Zhang, "Research on dtc system with variable flux for switched reluctance motor," *CES Trans. Elect. Machines Syst.*, vol. 1, no. 2, pp. 199–206, 2017.

[158] W. Zhang, L. Han, S. Wang *et al.*, "Minimising torque ripple of srm by applying db-dtfc," *IET Electric Power Appl.*, vol. 13, no. 11, pp. 1883–1890, 2019.

[159] N. Yan, X. Cao, and Z. Deng, "Direct torque control for switched reluctance motor to obtain high torque-ampere ratio," *IEEE Trans. Ind. Electron.*, vol. 66, no. 7, pp. 5144–5152, Jul. 2019.

[160] X. Sun, J. Wu, G. Lei, Y. Guo, and J. Zhu, "Torque ripple reduction of srm drive using improved direct torque control with sliding mode controller and observer," *IEEE Trans. Ind. Electron.*, to be published, doi: 10.1109/TIE.2020.3020026.

[161] H. Peyrl, G. Papafotiou, and M. Morari, "Model predictive torque control of a switched reluctance motor," in *Proc. IEEE Int. Conf. Ind. Technol.*, 2009, pp. 1–6.

[162] J. Villegas, S. Vazquez, J. Carrasco, and I. Gil, "Model predictive control of a switched reluctance machine using discrete space vector modulation," in *Proc. IEEE Int. Symp. Ind. Electron.*, 2010, pp. 3139–3144.

[163] H. Hu, X. Cao, N. Yan, and Z. Deng, "A new predictive torque control based torque sharing function for switched reluctance motors," in *Proc. 22nd Int. Conf. Elect. Machines Syst.*, 2019, pp. 1–5.

[164] S. Song, R. Hei, R. Ma, and W. Liu, "Model predictive control of switched reluctance starter/generator with torque sharing and compensation," *IEEE Trans. Transport. Electrific.*, vol. 6, no. 4, pp. 1519–1527, Dec. 2020.

[165] C. Li, G. Wang, Y. Li, and A. Xu, "An improved finite-state predictive torque control for switched reluctance motor drive," *IET Electric Power Appl.*, vol. 12, no. 1, pp. 144–151, 2017.

[166] R. Tarvirdilu-Asl, S. Nalakath, B. Bilgin, and A. Emadi, "A finite control set model predictive torque control for switched reluctance motor drives with adaptive turn-off angle," in *Proc. IECON 45th Annu. Conf. IEEE Ind. Electron. Soc.*, vol. 1, 2019, pp. 840–845.

[167] C. Pollock and C.-Y. Wu, "Acoustic noise cancellation techniques for switched reluctance drives," *IEEE Trans. Ind. Appl.*, vol. 33, no. 2, pp. 477–484, Mar./Apr. 1997.

[168] C.-Y. Wu and C. Pollock, "Analysis and reduction of vibration and acoustic noise in the switched reluctance drive," *IEEE Trans. Ind. Appl.*, vol. 31, no. 1, pp. 91–98, Jan./Feb. 1995.

[169] J. Mahn, D. Williams, P. Wung, G. Horst, J. Lloyd, and S. Randall, "A systematic approach toward studying noise and vibration in switched reluctance machines: Preliminary results," in *Proc. IAS 31st Conf. Rec. IEEE Ind. Appl. Conf. IAS Ann. Meeting*, vol. 2, 1996, pp. 779–785.

[170] D. Panda and V. Ramanarayanan, "Reduced acoustic noise variable dc-bus-voltage-based sensorless switched reluctance motor drive for hvac applications," *IEEE Trans. Ind. Electron.*, vol. 54, no. 4, pp. 2065–2078, Aug. 2007.

[171] M. L. M. Kimpara *et al.*, "Active cancellation of vibration in switched reluctance motor using mechanical impulse response method," *IEEE Trans. Energy Convers.*, vol. 34, no. 3, pp. 1358–1368, Sep. 2019.

[172] S. A. Long, Z. Zhu, and D. Howe, "Effectiveness of active noise and vibration cancellation for switched reluctance machines operating under alternative control strategies," *IEEE Trans. Energy Convers.*, vol. 20, no. 4, pp. 792–801, Dec. 2005.

[173] H. Makino, T. Kosaka, and N. Matsui, "Digital pwm-control-based active vibration cancellation for switched reluctance motors," *IEEE Trans. Ind. Appl.*, vol. 51, no. 6, pp. 4521–4530, Nov.-Dec. 2015.

[174] A. Tanabe and K. Akatsu, "Vibration reduction method in srm with a smoothing voltage commutation by PWM," in *Proc. 9th Int. Conf. Power Electron.*, 2015, pp. 600–604.

[175] J.-W. Ahn, S.-J. Park, and D.-H. Lee, "Hybrid excitation of srm for reduction of vibration and acoustic noise," *IEEE Trans. Ind. Electron.*, vol. 51, no. 2, pp. 374–380, Apr. 2004.

[176] S. Shin, N. Kawagoe, T. Kosaka, and N. Matsui, "Study on commutation control method for reducing noise and vibration in srm," *IEEE Trans. Ind. Appl.*, vol. 54, no. 5, pp. 4415–4424, Sep.-Oct. 2018.

[177] R. Pupadubsin, B. C. Mecrow, J. D. Widmer, and A. Steven, "Smooth voltage pwm for vibration and acoustic noise reduction in switched reluctance machines," *IEEE Trans. Energy Convers.*, to be published, doi: 10.1109/TEC.2020.3044917.

[178] A. D. Callegaro, B. Bilgin, and A. Emadi, "Radial force shaping for acoustic noise reduction in switched reluctance machines," *IEEE Trans. Power Electron.*, vol. 34, no. 10, pp. 9866–9878, Oct. 2019.

[179] M. Takiguchi, H. Sugimoto, N. Kurihara, and A. Chiba, "Acoustic noise and vibration reduction of srm by elimination of third harmonic component in sum of radial forces," *IEEE Trans. Energy Convers.*, vol. 30, no. 3, pp. 883–891, Sep. 2015.

[180] J. Furqani, M. Kawa, K. Kiyota, and A. Chiba, "Current waveform for noise reduction of a switched reluctance motor under magnetically saturated condition," *IEEE Trans. Ind. Appl.*, vol. 54, no. 1, pp. 213–222, Jan./Feb. 2018.

[181] N. Kurihara, J. Bayless, H. Sugimoto, and A. Chiba, "Noise reduction of switched reluctance motor with high number of poles by novel simplified current waveform at low speed and low torque region," *IEEE Trans. Ind. Appl.*, vol. 52, no. 4, pp. 3013–3021, Jul./Aug. 2016.

[182] J. Bayless, N. Kurihara, H. Sugimoto, and A. Chiba, "Acoustic noise reduction of switched reluctance motor with reduced rms current and enhanced efficiency," *IEEE Trans. Energy Convers.*, vol. 31, no. 2, pp. 627–636, Jun. 2016.

[183] J. Furqani, M. Kawa, C. A. Wiguna, N. Kawata, K. Kiyota, and A. Chiba, "Current reference selection for acoustic noise reduction in two switched reluctance motors by flattening radial force sum," *IEEE Trans. Ind. Appl.*, vol. 55, no. 4, pp. 3617–3629, Jul./Aug. 2019.

[184] M. Kawa, K. Kiyota, J. Furqani, and A. Chiba, "Acoustic noise reduction of a high-efficiency switched reluctance motor for hybrid electric vehicles with novel current waveform," *IEEE Trans. Ind. Appl.*, vol. 55, no. 3, pp. 2519–2528, May/Jun. 2019.

[185] J. Furqani, C. A. Wiguna, A. Chiba, O. Gundogmus, M. Elamin, and Y. Sozer, "Analytical and experimental verification of novel current waveforms for noise reduction in switched reluctance motor," in *Proc. IEEE Int. Electric Machines Drives Conf.*, 2019, pp. 576–583.

[186] J. Furqani, C. A. Wiguna, A. Chiba, O. Gundogmus, Y. Sozer, and A. Purwadi, "Experimental verification of acoustic noise and radial force sum variation in switched reluctance motor," *IEEE Trans. Ind. Appl.*, to be published, doi: 10.1109/TIA.2021.3066955.

[187] R. Zhong, X. Guo, M. Zhang, D. Ding, and W. Sun, "Influence of switch angles on second-order current harmonic and resonance in switched reluctance motors," *IET Electric Power Appl.*, vol. 12, no. 9, pp. 1247–1255, 2018.

[188] O. Gundogmus *et al.*, "Current profile optimization method for simultaneous dc-link current ripple and acoustic noise minimization in switched reluctance machines," in *Proc. IEEE Energy Convers. Congr. Expo.*, 2020, pp. 5574–5579.

[189] B. Fahimi, G. Suresh, K. Rahman, and M. Ehsani, "Mitigation of acoustic noise and vibration in switched reluctance motor drive using neural network based current profiling," in *Proc. 33rd Conf. Rec. IEEE Ind. Appl. Conf. IAS Annu. Meeting*, vol. 1, 1998, pp. 715–722.

[190] O. Gundogmus, M. Elamin, Y. Sezer, and A. Chiba, "Simultaneous torque and radial force ripple control for reduction of acoustic noise and vibration in switch reluctance machines," in *Proc. IEEE Energy Convers. Congr. Expo.*, 2018, pp. 722–728.

[191] A. D. Callegaro, B. Bilgin, and A. Emadi, "Radial force shaping for acoustic noise reduction in switched reluctance machines," *IEEE Trans. Power Electron.*, vol. 34, no. 10, pp. 9866–9878, Oct. 2019.

[192] A. Hofmann, A. Al-Dajani, M. Bösing, and R. W. De Doncker, "Direct instantaneous force control: A method to eliminate mode-0-borne noise in switched reluctance machines," in *Proc. Int. Elect. Machines Drives Conf.*, 2013, pp. 1009–1016.

[193] A. Hofmann and R. De Doncker, "Hysteresis-based DIFC in SRM: eliminating switching harmonics while improving inverter efficiency," *Proc. 7th IET Int. Conf. Power Electron., Machines Drives*, 2014, pp. 1–6.

[194] M. Zhang, I. Bahri, X. Mininger, and C. Vlad, "A new vibration reduction control strategy of switched reluctance machine," in *Proc. IEEE Int. Electric Machines Drives Conf.*, 2017, pp. 1–6.

[195] A. Klein-Hessling, A. Hofmann, and R. W. De Doncker, "Direct instantaneous torque and force control: A control approach for switched reluctance machines," *IET Elect. Power Appl.*, vol. 11, no. 5, pp. 935–943, 2017.

[196] A. Klein-Hessling, A. Hofmann, and R. W. De Doncker, "Direct instantaneous torque and force control: A novel control approach for switched reluctance machines," in *Proc. IEEE Int. Elect. Machines Drives Conf.*, 2015, pp. 922–928.

[197] M. Zhang, I. Bahri, X. Mininger, C. Vlad, H. Xie, and E. Berthelot, "A new control method for vibration and noise suppression in switched reluctance machines," *Energies*, vol. 12, no. 8, 2019, Art. no. 1554.

[198] M. Zhang, I. Bahri, X. Mininger, C. Vlad, and E. Berthelot, "Vibration reduction control of switched reluctance machine," *IEEE Trans. Energy Convers.*, vol. 34, no. 3, pp. 1380–1390, Sep. 2019.

[199] M. Zhang *et al.*, "Vibration reduction controller for a switched reluctance machine based on hw/sw partitioning," *IEEE Trans. Ind. Informat.*, vol. 17, no. 6, pp. 3879–3889, Jun. 2021.

[200] A. Hofmann, A. Klein-Hessling, I. Ralev, and R. De Doncker, "Measuring srm profiles including radial force on a standard drives test bench," in *Proc. IEEE Int. Electric Machines Drives Conf.*, 2015, pp. 383–390.

GAOLIANG FANG (Student Member, IEEE) received the B.S. and M.S. degree in electrical engineering from Northwestern Polytechnical University, Xi'an, China, in 2015 and 2018, respectively. He is currently working toward the Ph.D. degree in electrical engineering with McMaster Automotive Resource Center, McMaster University, Hamilton, ON, Canada. His research interests include torque control, vibration and noise reduction of switched reluctance machines and sensorless control for permanent magnet synchronous machine.

FILIPE P. SCALCON (Student Member, IEEE) received the B.Sc. and M.Sc. degrees in electrical engineering from the Federal University of Santa Maria (UFSM), Santa Maria, Brazil, in 2017 and 2019, respectively. He is currently working toward the Dr. Eng. degree with the Power Electronics and Control Research Group, UFSM. His research interests include electrical machine drives, renewable energy conversion, reluctance machines, and digital control.

DIANXUN XIAO (Student Member, IEEE) received the B.Eng. and M.Eng. degrees in electrical engineering from the Harbin Institute of Technology, Harbin, China, in 2016 and 2018, respectively. He is currently working toward the Ph.D. degree in electrical engineering with McMaster Automotive Resource Centre, McMaster University, Hamilton, ON, Canada.

His current research interests include permanent magnet synchronous motor drives, switched reluctance motor drives, high-power converters, and battery management systems.

RODRIGO P. VIEIRA (Member, IEEE) received the B.S. degree in electrical engineering from the Universidade Regional do Noroeste do Estado do Rio Grande do Sul, Ijuí, Brazil, in 2007, and the M.Sc. and Dr. Eng. degrees in electrical engineering from the Federal University of Santa Maria (UFSM), Santa Maria, Brazil, in 2008 and 2012, respectively. From 2010 to 2014, he was with the Federal University of Pampa, Alegrete, Brazil. Since 2014, he has been with the UFSM, where he is currently a Professor. His research interests include electrical machine drives, sensorless drives, digital control techniques of static converters, and energy systems.

HILTON A. GRÜNDLING (Member, IEEE) was born in Santa Maria, Brazil, in 1954. He received the B.Sc. degree from the Pontifical Catholic University of Rio Grande do Sul, Porto Alegre, Brazil, in 1977, the M.Sc. degree from the Federal University of Santa Catarina, Santa Catarina, Brazil, in 1980, and the D.Sc. degree from the Technological Institute of Aeronautics, São Paulo, Brazil, in 1995. Since 1980, he has been with the Federal University of Santa Maria, Rio Grande do Sul, Brazil, where he is currently a Titular Professor. His research interests include robust model reference adaptive control, discrete control, and control system applications.

ALI EMADI (Fellow, IEEE) received the B.S. and M.S. degrees in electrical engineering with highest distinction from the Sharif University of Technology, Tehran, Iran, in 1995 and 1997, respectively, and the Ph.D. degree in electrical engineering from Texas A&M University, College Station, TX, USA, in 2000. He is currently the Canada Excellence Research Chair Laureate with McMaster University, Hamilton, ON, Canada. He is also the holder of the NSERC/FCA Industrial Research Chair of Electrified Powertrains and Tier I Canada Research Chair of transportation electrification and smart mobility. Before joining McMaster University, he was the Harris Perlstein Endowed Chair Professor of engineering and Director of the Electric Power and Power Electronics Center and Grainger Laboratories, Illinois Institute of Technology, Chicago, IL, USA, where he established research and teaching facilities as well as courses in power electronics, motor drives, and vehicular power systems. He was the Founder, Chairman, and President of Hybrid Electric Vehicle Technologies, Inc. (HEVT) – a university spin-off company of Illinois Tech. He is currently the President and Chief Executive Officer of Enedym Inc. and Menlolab Inc.–two McMaster University spin-off companies. He is the Principal author or coauthor of more than 500 journal and conference papers and several books including *Vehicular Electric Power Systems* (2003), *Energy Efficient Electric Motors* (2004), *Uninterruptible Power Supplies and Active Filters* (2004), *Modern Electric, Hybrid Electric, and Fuel Cell Vehicles* (2nd edition, 2009), and *Integrated Power Electronic Converters and Digital Control* (2009). He is also the Editor of the *Handbook of Automotive Power Electronics and Motor Drives* (2005) and *Advanced Electric Drive Vehicles* (2014). He is the co-editor of the *Switched Reluctance Motor Drives* (2018). He was the Inaugural General Chair of the 2012 IEEE Transportation Electrification Conference and Expo (ITEC) and has chaired several IEEE and SAE conferences in the areas of vehicle power and propulsion. From 2014 to 2020, he was the founding Editor-in-Chief of the IEEE TRANSACTIONS ON TRANSPORTATION ELECTRIFICATION.